Science
AAAS

Supplementary Materials for

Human TKTL1 implies greater neurogenesis in frontal neocortex of modern humans than Neanderthals

Anneline Pinson *et al*.

Corresponding author: Wieland B. Huttner, huttner@mpi-cbg.de

Science **377**, eabl6422 (2022)
DOI: 10.1126/science.abl6422

The PDF file includes:

Other Supplementary Material for this manuscript includes the following:

Materials and Methods

Lead contact and materials availability

Further information and requests for resources and reagents should be directed to, and will be fulfilled by, the Lead Contact, Wieland B. Huttner (huttner@mpi-cbg.de). All unique/stable reagents generated in this study are available from the Lead Contact with a completed Materials Transfer Agreement.

Experimental animals

All animal experimental procedures were performed in accordance with the German Animal Welfare Legislation ("Tierschutzgesetz") after approval by the federal state authority Landesdirektion Sachsen (licenses: TVV 2015/05, TVV13/2020, TVV21/2017). All procedures were overseen by the Institutional Animal Welfare Officer. All animals used for this study were kept in standardized pathogen-free conditions at the Biomedical Services Facility (BMS) of MPI-CBG with free access to food and water. Mice were kept in a 12 hours/12 hours light/dark cycle, and ferrets were kept in a 16 hours/8 hours light/dark cycle. As the gender of embryos is unlikely to influence the results obtained in the present study, it was not taken into consideration. The C57BL/6JOlaHsd mouse line was bred at the BMS of MPI-CBG. Timed pregnant ferrets (Mustela putorius furo) were obtained from Marshall BioResources (NY, USA) and housed at the BMS of MPI-CBG.

Human tissue

Fetal human neocortex tissue (PCW 8-14) was obtained (i) from the Klinik und Poliklinik für Frauenheilkunde und Geburtshilfe, Universitätsklinikum Carl Gustav Carus of the Technische Universität Dresden, with informed written maternal consent, and with approval of the local University Hospital Ethical Review Committees; and (ii) from the Human Development Biology Resource (HDBR), with the fetal human material being provided by the joint MRC/Welcome Trust (MR/R006237/1) Human Developmental Biology Resource (https://www.hdbr.org). Tissue obtained from Dresden was dissected in PBS and cultured in human slice culture medium (hSCM, see below) for 2 hours before any manipulation. Tissue obtained from the HDBR was shipped in Hibernate E media (GIBCO A12476601) and cultured in hSCM for 3 to 5 hours prior to any further manipulation. The age of fetuses was assessed by ultrasound measurements of crown-rump length and other standard criteria of developmental stage determination. PCW 8-14 corresponds to a mid-neurogenesis stage. Due to protection of data privacy, the gender of the human fetuses from which neocortical tissue was obtained cannot be reported. The gender is unlikely to influence the results obtained in the present study.

Plasmids

hTKTL1-encoding cDNA (short isoform) was amplified by PCR from a human brain cDNA library and cloned into a pCAGGS vector (*22*) to obtain pCAGGS-hTKTL1. The aTKTL1 plasmid was obtained by mutation of hTKTL1 using the Quick-change Lightning Site-Directed Mutagenesis kit (Agilent). pCAGGS-GFP and pCAGGS-mCherry have previously been published (*22, 44*). All plasmids were extracted and purified using the QIAEX II Gel Extraction Kit (QIAGEN), eluted in 20 µl of distilled water, and then used to transform competent cells. Subsequently, all plasmids were extracted and purified using the Plasmid Plus Maxi kit (QIAGEN) following the manufacturer's instructions.

In utero electroporation of embryonic mouse neocortex

IUE was performed as previously described (*31*). Pregnant mice carrying E13.5 (for lateral neocortex IUE) or E15.5 (for medial neocortex IUE) embryos were anesthetized with 4% isoflurane (Baxter, HDG9623) in a narcosis box, followed by a constant 2.5% isoflurane flow during the procedure. The animals were injected subcutaneously with an analgesic (0.1 ml, Metamizol, 200 mg/kg). Using a borosilicate microcapillary (Sutter instruments, BF120-69-10), the embryos were injected intraventricularly with a solution containing 0.1% Fast Green (Sigma) in PBS, 1 µg/µl of pCAGGS plasmid (either empty vector, hTKTL1, aTKTL1) and 0.4 µg/µl or 1 µg/µl (for cell sorting) of pCAGGS-GFP. The embryos were then electroporated using a 3-mm diameter electrode (26 V, six 50-msec pulses with 950-msec intervals), with the anode and cathode positioned adequately to promote DNA entry into either the lateral or medial neocortex. After the IUE, the peritoneum was sutured (VICRYL 5-0, V493H), and the abdominal skin was closed with clips (BD, Autoclip 9 mm, 427631). After surgery animals received Metamizol for two days via the drinking water (1.33 mg/ml). Pregnant mice were sacrificed by cervical dislocation, and embryos were immediately harvested and sacrificed by decapitation at E15.5 or E17.5 (for lateral neocortex IUE) or at E18.5 (for medial neocortex IUE). The embryonic brains were dissected and either fixed with 4% paraformaldehyde in 120 mM phosphate buffer pH 7.4 (PFA-PB), overnight at 4˚C, for immunofluorescence, or used for hemisphere rotation culture or cell sorting (see below).

In utero electroporation of embryonic ferret neocortex

E33 ferret neocortex was electroporated as described previously (*44*). Pregnant ferrets (with embryos at E33) were anesthetized with 4% isoflurane in a narcosis box before being placed on the operation table under 3 ± 0,5% isoflurane anesthesia. Pregnant ferrets were injected subcutaneously with an analgesic (0.1 ml Metamizol, 50 mg/kg, WDT), an antibiotic (0.13 ml amoxicillin, 20 mg/kg, WDT) and glucose (10 ml of a 5% D-glucose solution). The uterus was exposed and the embryos were injected intraventricularly with 0.1% Fast Green (Sigma) in PBS, 2.5 µg/µl of either empty pCAGGS (control) or pCAGGS-hTKTL1, and 1 µg/µl of either pCAGGS-GFP or pCAGGS-mCherry. The plasmids encoding the two different fluorescent proteins were used in order to be able to discern the control and the hTKTL1-electroporated postnatal pups. pCAGGS-GFP and pCAGGS-mCherry were alternated for different pregnant ferrets. The injected embryos were electroporated with six 50-msec pulses of 100 V at 1-sec intervals. The ferrets were sutured (VICRYL 4-0, VCP392ZH), then monitored until they woke up, and then had postoperative care for at least 2 days (1 x daily 20 mg/kg amoxicillin and 3 x daily 50 mg/kg Metamizol). Following birth, the pups were sacrificed at P2 or P16. At P2, pups were anesthetized by intraperitoneal injection of 4 mg/kg xylazine and 40 mg/kg of ketamine. When in deep anesthesia, the pups were sacrificed by decapitation and the brains isolated. The brains were fixed in PFA-PB at 4˚C for 48 hours. At P16 the anesthesia was followed by intracardiac perfusion with PBS and then with PFA-PB. The brains were isolated and fixed with PFA-PB at 4˚C for 48 hours. Post-delivery ferrets underwent a second surgery for ovariohysterectomy. A minimum of 2 weeks after the latter surgery, the ferrets were donated for adoption.

Mouse cerebral hemisphere rotation culture

Cerebral hemispheres were dissected from E14.5 mouse embryos 24 hours after IUE at E13.5. Meninges were surgically removed, and the electroporated hemispheres were placed into

hemisphere rotation (HERO) culture as previously described (*45*), with minor modifications. Hemispheres were cultured with mouse slice culture medium (mSCM), which had the following composition: a mixture of 90% neurobasal medium (GIBCO, 21103049) and 10% rat serum (Charles River japan) was supplemented with 20 mM L-glutamine, 1x Penstrep, 1x N2 supplement (GIBCO, 17502048), 1x B27 supplement (GIBCO, 17504044) and 0.1 mM HEPES-NaOH (pH 7.3). Cerebral hemispheres were placed into a flask (for the whole-embryo culture incubator, see below) containing 1.5 ml of mSCM containing 0.1% DMSO and either (i) no further addition (control), (ii) 10, 50 or 100 µM of 6-aminonicotinamide (6-AN, Sigma, A68203) (*34*), (iii) 10 or 20 µM of S3 (Ambeed, 5539-66-2) (*49*), (iv) 10, 20 or 50 µM of 5-(tetradecyloxy)-2-furoic acid (TOFA, Sigma, T6575) (*50*), (v) 5 µM of ND646 (MedChemExpress, HY-101842) (*51*) or (vi) 5, 10, 20 µM of Orlistat (Sigma, O4139) (*52*) as indicated in the figures. The flasks were incubated for 24 hours at 37˚C in a whole-embryo culture incubator (Ikemoto Scientific Technology), with a humidified atmosphere of 40% O2 / 5% CO2 / 55% N2 and under rotation at 6 rpm. The cerebral hemispheres were then fixed overnight with PFA-PB at 4˚C for immunofluorescence.

Human neocortex free-floating tissue culture

Free-floating tissue (FFT) culture of fetal human neocortical tissue (PCW 8-14) was performed for 48 hours (inhibitors) or 72 hours (CRISPR/Cas9 KO) as previously described (*46*). FFT was performed using hSCM, which had the following composition: a mixture of 90% neurobasal medium (GIBCO, 21103049) and 10% of knockout serum replacement (KOSR, GIBCO, 10828028) was supplemented with 20 mM L-glutamine, 1x Penstrep, 1x N2 supplement (GIBCO, 17502048), 1x B27 supplement (GIBCO, 17504044) and 0.1 mM HEPES-NaOH (pH 7.3). For the pharmacological inhibitor studies, fetal human neocortical tissue was placed into a flask containing 1.5 ml of hSCM containing 0.1% DMSO and either (i) no further addition (control), (ii) 10, 20, 50 or 100 µM of 6-AN (Sigma, A68203), (iii) 5, 10 or 20 µM of S3 (Ambeed, 5539-66-2), (iv) 10, 20 or 50 µM of TOFA (Sigma, T6575), (v) 5 µM of ND646 (MedChemExpress, HY-101842) or (vi) 5, 10, 20 µM of Orlistat (Sigma, O4139) as indicated in the figures. The flasks were incubated for 48 or 72 hours at 37˚C in a whole-embryo culture incubator (Ikemoto Scientific Technology), with a humidified atmosphere of 60% O2 / 5% CO2 / 35% N2 and under rotation at 6 rpm. Cultures received fresh hSCM (containing the above ingredients) every 24 hours. The fetal human neocortical tissue was then fixed overnight with PFA-PB at 4˚C for immunofluorescence.

CRISPR/Cas9 strategy for hTKTL1 knockout in human fetal neocortical tissue

The CRISPR/Cas9 approach used to perform a knockout (KO) of hTKTL1 expression in human fetal neocortical tissue ex vivo was similar to the previously reported approaches (*31, 53*). As control, a previously published gRNA targeting LacZ was used (*53*). The genomic sequence of hTKTL1 was analyzed for CRISPR/Cas9 target sites (Geneious 11 software, Biomatters), and 3 gRNAs were selected (gRNAs 1-3, gRNA-1: 5'-CTTACAGAGACTGTCGTTTG-3', gRNA-2: 5'-ATACTGGCAAGTACTTCGAC-3', gRNA-3: 5'-GGATGGCTCGGACAAGGACT-3'). gRNAs and recombinant HF-Cas9 V3 protein generated by Integrated DNA Technologies (IDT) were used. The gRNAs were tested in combinations of two gRNAs each by electroporation of HeLa cells followed by genomic PCR analysis (forward primer: 5'-GGACGCTGCTACAGAGCTGA-3', reverse primer: 5'-TCCACATCACGGAGATAGGTG). As all three combinations of gRNAs cut hTKTL1, the combination with the greatest efficiency (gRNA-2 plus gRNA-3) was chosen (Fig. S8H). A gRNA–tracrRNA duplex was prepared for each

gRNA (1 µl of 100 µM gRNA and 1 µl of 100 µM tracr) and incubated for 5 min at 95˚C. Once at room temperature, 1 µl of lacZ gRNA or 0.5 µl of gRNA-2 plus 0.5 µl of gRNA-3 were mixed with 0.6 µl of HF-Cas9 V3 protein and incubated at room temperature for 15 min. Each Cas9-gRNA complex was then diluted into 18.4 µl of 1.1x protein buffer (20 mM Hepes pH 7.5, 150 mM KCl), followed by centrifugation (1 min, 10,000x g) through a PVDF 0.22 µm filter.

Ex vivo electroporation of human fetal neocortical tissue

Ex vivo electroporation of human fetal neocortical tissue was performed as previously described (*39*). Briefly, neocortical tissue was placed in a spoon-shaped anode filled with sterile PBS. A mixture of either the Cas9–LacZ-gRNA complex (control) or the Cas9–hTKTL1-gRNA complex, 0.1% Fast Green, 0.7 µg/µl of pCAGGS-GFP and 4% glycerol was added onto the apical surface of the human fetal neocortical tissue. The cathode was placed above the tissue, which was then electroporated using five 50-msec pulses at 36-40 V with 950-msec intervals. The tissue was then washed in PBS and transferred to a flask for a 72-hour FFT culture. The cultures received fresh hSCM every 24 hours. The fetal human neocortical tissue was then fixed overnight in PFA-PB at 4˚C for immunofluorescence.

CRISPR-Cas9 editing of H9 human embryonic stem cells

H9 human embryonic stem cells (female, WiCell Research Institute, ethics permit AZ 3.04.02/0118) were grown on Matrigel (Corning, 35248) in mTeSR1 medium (StemCell Technologies, 05852). Electroporation of oligonucleotides and ribonucleoprotein (RNP) was carried out using 1 million cells, 100 pmol electroporation enhancer (IDT), 320 pmol gRNA (crRNA/tracR duplex), 200 pmol single-stranded (ss)DNA donor, and 252 pmol Cas9-HiFi (IDT) using the B-16 program of the Nucleofector 2b Device (Lonza) in cuvettes for 100 µl Human Stem Cell nucleofection buffer (Lonza, VVPH-5022). Cells were counted with Countess automated cell counter (Invitrogen). To increase HDR, 2 µM M3814 was added for two days after electroporation (*54*).

TKTL1_t1_guide sequence: CTCAGAGAAAGTAGAGTACC
TKTL1_ssDNA donor (edited site bold):
TAGATAGCTACTCGGAAAGCATGCGGTCTGGCTCTGGCTAAGCTGGGCTACGCGAA
CAACAGAGTCGTTGTGCTGGATGGTGACACCAAGTACTCTACTTTpTATTCAACAAG
GAGTACC

Validation of edited cell lines. Genomic DNA of each single cell-derived cellular clone was isolated using QuickExtract DNA Extraction Solution (Lucigen), before a region of ~250 bp around the cut site was amplified and sequenced using the primers:

TKTL1_NGS_forward:
ACACTCTTTCCCTACACGACGCTCTTCCGATCTCCTTCCTTCTGTAGTCGTTCC
TKTL1_NGS_reverse:
GTGACTGGAGTTCAGACGTGTGCTCTTCCGATCTCCAGTGGGCCATTGATTCTA

From sequences the editing state was evaluated as described (*54*). Briefly, deletions bigger than ~250 bp and therefore not detected by the amplicon sequencing (*37, 55*) were identified by digital droplet (dd)PCR using primer pairs and probes that anneal within the sequenced target

regions. The master mix for ddPCR amplification included 1× ddPCR Supermix for probes (no dUTP, Bio-Rad), 0.2 µM of each primer and 0.2 µM probe (both IDT) for target and reference, together with 1 µl genomic DNA isolate. After droplet generation with the QX200 Droplet generator (Biorad), the PCR reaction parameters were: 5 min at 95°C, followed by 40 cycles of 30 sec at 95°C (ramp rate of 2°C/sec), 60 sec at 59°C (ramp rate of 2°C/sec), and 5 min at 98°C. Readout was in a QX200 Droplet reader (BioRad) and allele copy numbers were determined relative to a different fluorophore for the FOXP2 reference and unedited control.

The following primers and probes were used:
TKTL1_ddPCR_forward: CTACCACCTGATTGTCTCTGT
TKTL1_ddPCR_reverse: AGAAGCCCTGAGAGACACTA
TKTL1_ddPCR_probe: 6FAM –CGGTCTGGCTCTGGCTAAGCTGGGC- BHQ_1

FOXP2_ddPCR_forward: GCAACAGCAATTGGCAGC
FOXP2_ddPCR_reverse: CAGCGATTGGACAGGAAGTG
FOXP2_ddPCR_probe: HEX –AGCAGCAGCAGCATCTGCTCAGCCT- BHQ_1

To exclude cellular clones with a loss-of-heterozygosity at the region near the CRISPR cut site (*55*), heterozygous variable positions upstream and downstream of the respective target site were amplified and sequenced using the primers:

TKTL1_downSNP_forward:
ACACTCTTTCCCTACACGACGCTCTTCCGATCTCCTTAGCCTCCCGAGTAGCT
TKTL1_downSNP_reverse:
GTGACTGGAGTTCAGACGTGTGCTCTTCCGATCTAAATACACCATCGGGCTGGG
TKTL1_upSNP_forward:
ACACTCTTTCCCTACACGACGCTCTTCCGATCTAGGGAGGTGGCTCTAGAAGT
TKTL1_upSNP_reverse:
GTGACTGGAGTTCAGACGTGTGCTCTTCCGATCTAGCAAGGTGGTGGCCAAG

To detect chromosomal aneuploidies and large-scale chromosomal duplications and deletions, DNA from the two mock-edited and the two aTKTL1-edited H9 human embryonic stem cell (ESC) lines was sequenced shallowly as described in Riesenberg et al. 2019 (*54*), and the result compared to that of the shallowly sequenced DNA from their mother H9 line (Fig S7C).

Karyotyping

The karyotypes of the H9 human ESC lines (hTKTL1–1, hTKTL1–2, aTKTL1–1, aTKTL1–2) were obtained by Giemsa-banding (GTG banding) and performed at the Institute of Clinical Genetics of the Technische Universität Dresden, which is accredited by DIN EN ISO 15189:2014. In short, cells were incubated for 3 h with 10 µg/ml colcemid (Gibco, 15212012) and trypsinized (Gibco 25300054) to obtain a single cell suspension. The cell suspensions were then treated with hypotonic 0.075 M KCl Solution (Gibco, 10575090) and subsequently fixed with 3:1 methanol/acetic acid (Merck). Cells were then spread onto glass slides and treated with the Giemsa (GTG) staining procedure from Thermo Fisher (Cat. No. 10582013, 10092013 and 15090046) (https://www.thermofisher.com/de/en/home/references/protocols/cell-and-tissue-analysis/staining-protocol/giemsa-banding.html.).

Pluripotency analysis

H9 human ESC lines were analyzed for pluripotency by immunofluorescence for pluripotency markers and flow cytometry of the immunostained cells. The H9 human ESC lines (hTKTL1–1, hTKTL1–2, aTKTL1–1, aTKTL1–2) were grown on coverslips and fixed with PFA-PB for 20 min at room temperature. The cells were washed three times with PBS. The cells were permeabilized three times 15 min with 0.1% Triton X-100 in PBS and then subjected to blocking for 30 min in 0.1% Triton X-100 and 4% donkey serum, in PBS (blocking solution). The primary antibodies were incubated in blocking solution overnight at 4˚C. The primary antibodies used were mouse anti-Nanog-PE-conjugated antibody (1:10) and mouse anti-Oct3/4-PerCy5.5-conjugated antibody (1:10) from the Human pluripotent stem cell transcription factor analysis kit (560589, BD), rat anti-SSEA3-PE-conjugated antibody (1:10) from the Human pluripotent stem cell sorting and analysis kit (560461, BD) or mouse anti-Sox2 (MAB2018, R&D, clone 245610, RRID:AB_358009, 1:200). Subsequently, the cells were washed three times in blocking solution and incubated with secondary antibody (for the unconjugated Sox2 antibody, donkey anti-mouse, Alexa Fluor 488 (Cat #A21202, RRID:AB_141607, 1:500)), and DAPI (Sigma, 1:1000) in blocking solution for 1 hour at room temperature. The sections were then washed three times with blocking buffer, three times with PBS and one time with H_20 before being mounted with Mowiol.

For the flow cytometry analyses, we first prepared a single-cell suspension from the H9 human ESC lines (hTKTL1–1, hTKTL1–2, aTKTL1–1, aTKTL1–2). To this end, the cells were washed with PBS before using TrypLE (12604013, Gibco) for 4 min. mTeSR1 medium was added to the cells that were then collected by pipetting up and down. The cell suspension was subjected to fixation and staining. The cells were centrifuged at 300xg for 3 min, the supernatant was removed and the cells were fixed with PFA-PB for 20 min at room temperature before being washed three times with PBS. The cells were permeabilized three times 15 min with 0.1% Triton X-100 in PBS, and blocked for 30 min with 0.1% Triton X-100 and 5% FBS in PBS. Then 100 µl of cell suspension were incubated overnight at 4˚C with the following antibodies (1:6): mouse anti-Nanog-PE-conjugated antibody, mouse anti-Oct3/4-PerCy5.5-conjugated antibody, mouse anti-Sox2-Alexa Fluor 647 conjugated antibody from the Human pluripotent stem cell transcription factor analysis kit (560589, BD). Subsequently, the cells were washed three times 15 min in 0.1% Triton X-100 in PBS and resuspended in 200 µl PBS. The cells were then analyzed using a BD FACSAria 3 device (Becton Dickinson Biosciences). Gates were applied as follows. First, a P1 gate was set on the SSC-A/FSC-A dot-plot, to identify live cells based on size and shape. Next, the P1 fraction was restricted by setting a P2 gate on the FSC-W/FSC-H dot-plot to select single cells. Out of the P2 population, single dot-plots were created for FSC-H/PE, FSC-H/APC and FSC-H/PerCP-Cy5-5-A. Dot-plots and histograms were created in the FL channels. Data were analyzed using the FlowJo software.

Cerebral organoids

Two mock-edited (hTKTL1) and two gene-edited (aTKTL1) H9 cell lines were cultivated on Matrigel– (Corning) coated tissue culture plates using standard feeder-free conditions in mTeSR1 (StemCell Technologies) and differentiated into cerebral organoids using previously published protocols (*47, 48*). Briefly, 9,000 cells were seeded per well into 96-well Ultra-low attachment plates (Corning) in mTeSR containing 10 µM Y27632 (AbMole), followed by centrifugation at 300x g for 3 min. After 48 hours the medium was changed to mTeSR without

Y27632. Four days after seeding, the medium was changed to neural induction medium, which contained DMEM/F12 (Gibco) medium supplemented with 1% N2 supplement (Gibco), 1% Glutamax supplement (Gibco), 1% MEM non-essential-amino acids (Gibco) and 1 μg/ml heparin (Sigma-Aldrich). The neural induction medium was changed every other day. Eight days after seeding, the embryoid bodies were embedded in Matrigel and transferred to differentiation medium (equal volumes of DMEM/F12 (Gibco) and Neuralbasal (Gibco) medium supplemented with 0.5% N2 supplement (Gibco), 0.025% insulin solution (Sigma-Aldrich), 1% Glutamax supplement (Gibco), 0.5% MEM non essential-amino-acids (Gibco), 1% B27 supplement (without vitamin A, Gibco), 1% penicillin-streptomycin and 0.00035% 2-mercaptoethanol (Merck)), and placed on an orbital shaker. The medium was changed every other day. On day 14 after seeding, the cerebral organoids were switched to differentiation medium containing 1% of B27 supplement with vitamin A (Gibco), which was changed every three days until fixation at day 50 with PFA-PB at 4°C for 2 hours.

Sanger sequencing and quantitative real-time PCR (qPCR)

Total RNA was isolated from day 50 mock-edited and gene-edited H9-derived human organoids using the RNAeasy Micro Plus Kit (Qiagen) according to the manufacturer's instructions. cDNA was synthesized using the Maxima first-strand cDNA synthesis kit (Thermo Scientific). The expression of TKTL1 mRNA in the mock-edited and gene-edited human organoids was confirmed by qPCR, using each of the cDNAs generated as template and specific primers (forward primer 5'- GCGGTCTGGCTCTGGCTAAG -3', reverse primer 5'- GCAAAAGCAATGGTCCGTCC -3'), followed by Sanger sequencing of the PCR products. The sequences obtained from the mock-edited and gene-edited organoids were mapped to the human TKTL1 gene, using Geneious (version 11.1.4). This revealed the expression of the human TKTL1 mRNA in the mock-edited human organoids (hTKTL1-1 and hTKTL1-2) and the expression of the archaic TKTL1 mRNA in the gene-edited human organoids (aTKTL1-1 and aTKTL1-2).

Cryosectioning

As described previously (*31*), fixed tissues were incubated with 15% sucrose for 24 hours (mouse and human) or 48 hours (ferret) at 4˚C, followed by incubation with 30% sucrose for 24 hours (mouse and human) or 48 hours (ferret) at 4˚C. The tissues were embedded in Tissue-Tek (Sakura Finetek, 4583). Coronal cryosections of 20-50 μm thickness were cut using a cryostat and stored at –20˚C, prior to immunofluorescence.

Immunofluorescence

As described previously (*29*), cryosections were subjected to antigen retrieval using 10 mM citrate buffer pH 6.0 at 70˚C in a waterbath, as follows: (i) a 1-hour incubation for all embryonic mouse samples and the P2 ferret samples, and (ii) a 30-min incubation for all fetal human samples. Cryosections were permeabilized with 0.3% Triton X-100 in PBS for 30 min at room temperature, then quenched with 0.1 M glycine in PBS for 30 min. The samples were then subjected to blocking for 30 min in 0.2% gelatin, 300 mM NaCl, 0.3% Triton X-100, all in PBS. Primary antibodies (see below) were incubated in blocking solution overnight at 4˚C. Subsequently, the cryosections were washed three times in blocking solution and incubated with secondary antibodies (see below) and DAPI (Sigma) in blocking solution for 1 hour at room temperature. The sections were then washed three times with PBS and mounted with Mowiol.

The following primary antibodies were used: mouse anti-pVim (MBL D076-3, RRID:AB_592963, 1:500), goat anti-Sox2 (R&D Systems, AF2018, RRID:AB_355110, 1:500), rabbit anti-Tbr2 (Abcam, ab183991, RRID:AB_2721040, 1:500), mouse anti-Satb2 (Abcam, ab51502, RRID:AB_882455, 1:500), rat anti-Ctip2 (Abcam, ab18465, RRID:AB_2064130, 1:500), mouse anti-PCNA (Millipore, CBL407, RRID:AB_93501, 1:500), mouse anti-TKTL1 (Santa Cruz, sc-271296, RRID:AB_10612386, 1:250), chicken anti-GFP (Aves labs, GFP-1020, RRID:AB_10000240, 1:1000), rat anti-RFP (ChromoTex, 5F8, RRID:AB_2336064, 1:500), rabbit anti-RFP (Rockland antibodies, 600-401-379, RRID:AB_2209751 1:1000), rat anti-PH3 (Abcam, ab10543, RRID:AB_2295065, 1/500), rabbit anti-active Caspase 3 (Abcam, ab2302, RRID:AB_302962, 1:250), Rabbit anti-NeuN (Abcam, ab104225, RRID:AB_10711153, 1:500), mouse anti-Hu (Thermo Fisher, A-21271, RRID:AB_221488, 1:500), rabbit anti-Hopx (Sigma, HPA030180, RRID:AB_10603770, 1:100).

The following secondary antibodies were used at 1:500: donkey anti-chicken Cy2 (Jackson Immuno research, 703-225-155, RRID:AB_2340370), donkey anti-mouse Cy3 (Jackson Immuno research, 715-165-150, RRID:AB_2340813), donkey anti-mouse Cy5 (Jackson Immuno research, 715-175-151, RRID:AB_2340820), donkey anti-mouse Cy2 (Jackson Immuno research, 715-225-150, RRID:AB_2340826), donkey anti-rabbit Cy2 (Jackson Immuno research, 711-225-152, RRID:AB_2340612), donkey anti-rabbit Cy3 (Jackson Immuno research, 711-165-152, RRID:AB_2307443), donkey anti-rabbit Cy5 (Jackson Immuno research, 711-175-152, RRID:AB_2340607), donkey anti-rat Cy2 (Jackson Immuno research, 712-225-153, RRID:AB_2340674) donkey anti-rat Cy3 (Jackson Immuno research, 712-165-153, RRID:AB_2340667), donkey anti-rat Cy5 (Jackson Immuno research, 705-175-153, RRID:AB_2340672), donkey anti-goat Cy5 (Jackson Immuno research, 712-175-147, RRID:AB_2340415).

Image acquisition

Most fluorescent images were acquired using a Zeiss LSM 880 upright single-photon point scanning confocal microscope. Only few images were acquired using a Zeiss LSM 700 inverted single-photon point scanning confocal microscope. The images were taken using a Zeiss Plan-Apochromat 10x 0.45 air, a Zeiss Plan-Apochromat 20x 0.8 air, or a Zeiss Plan-Apochromat 40x 1.2 water objectives. The images were taken as either 1-µm thick optical sections (40x), 2-µm thick optical sections (20x), or 7-µm thick optical sections (10x).

Isolation of bRG and determination of acetyl-CoA levels

We first prepared a single-cell suspension from embryonic mouse neocortex which was then subjected to cell-surface staining. To this end, mouse neocortices electroporated at E13.5 with 1 µg/µl of pCAGGS plasmid (either empty vector (control), hTKTL1 or aTKTL1) and 1 µg/µl of pCAGGS-GFP were microdissected at E15.5 under an epifluorescence stereomicroscope to obtain the electroporated region of the neocortex. Microdissected neocortices of each electroporation condition (control, hTKTL1 or aTKTL1; 4-10 microdissected neocortices per condition) were pooled and the three pools processed in parallel. Single-cell suspensions were prepared using the MACS Neural Tissue Dissociation kit containing papain (Miltenyi Biotec) following the manufacturer's instruction. Cell-surface staining of prominin-1 (Prom-1) and GLAST was performed on the cell suspensions with rat 13A4 APC-conjugated antibody (1:50, eBioscience,

Clone 13A4, #17-1331-81, RRID:AB_823120) and with anti-EAAT1/GLAST-1/SLC1A3 PE-conjugated antibody (1:20, Novus Biologicals, #NB100-1869PE).

Next, fluorescence-activated cell sorting (FACS) was performed using a 5-laser-BD FACSAria Fusion sorter (Becton Dickinson Biosciences). Cell suspensions were first washed twice with Hanks' Balanced Salt Solution (HBSS) before being subjected to FACS. Gates were applied as follows. First, a P1 gate was set on the SSC-A/FSC-A dot-plot, to identify live cells based on size and shape. Next, the P1 fraction was restricted by setting a P2 gate on the FSC-W/FSC-H dot-plot to select single cells. Out of the P2 population, single dot-plots were created for SSC-A/GFP (linear/log2, blue laser, 488 nm), SSC-A/PE (linear/log2, yellow-green laser, 561 nm) and SSC-A/APC (linear/log2, red laser, 640 nm), to visualize the fluorescence intensities of GFP, Prom-1-APC and GLAST-PE, respectively. Voltage parameters were set based on an unstained control, and subsequently maintained for FACS. Next, the GFP+/GLAST+/Prom-1– gate was restrictively set and maintained through FACS to acquire electroporated bRG, which were sorted at room temperature into 100 µl HBSS in Eppendorf tubes. Sorted bRG were briefly centrifuged at 1000x g for 5 min, resuspended in 20-40 µl acetonitrile, rapidly frozen on dry ice and then kept at –80°C until further analysis. Three independent experiments were conducted.

We used mass spectrometry to determine the acetyl-CoA level in the FACS-isolated bRG. To this end, the frozen sorted bRG suspension was thawed and 150 µl 30% methanol in acetonitrile containing 100 nM chloropropamide and 5 µM 13C/15N-labeled AMP (Merck 650676) as internal standards were added. The suspenion then received 1/3 volume of 0.5 mm zirconium beads, followed by homogenization for 10 min at 4°C and 300x g in a TissueLyser II (Qiagen). Next, 10 µl of the homogenate was used for protein quantification by the BCA Protein Quantification Kit (Pierce BCA Protein Assay Kit, Tehermo Scientific) to ascertain that the protein concentration was consistent with the number of cells in the three types of samples. The remainder of the homogenate was centrifuged at 13,000x g for 30 min and the supernatant transferred to a new tube. LC–MS/MS analysis was performed on a high performance liquid chromatography (HPLC) system (1200 Agilent) coupled online to G2-S QTOF (Waters). For normal phase chromatography, a Bridge Amide 3.5 µl (2.1x100mm) column from Waters was used. For the normal phase, the mobile phase composed of eluent A (95% acetonitrile, 0.1 mM ammonium acetate, and 0.01% NH4OH) and eluent B (40% acetonitrile, 0.1 mM ammonium acetate, and 0.01% NH4OH) was applied with the following gradient program: Eluent B, from 0% to 100% within 18 min; 100% from 18 to 21 min; 0% from 21 to 26 min. The flow rate was set at 0.3 ml/min. The spray voltage was set at 3.0 kV and the source temperature was set at 120°C. Nitrogen was used as both cone gas (50 l/h) and desolvation gas (800 l/h), and argon as the collision gas. MSE mode was used in negative ionization polarity. Chromatograms and mass spectral data were acquired and processed by MassLynx software (Waters). The acetyl-CoA peak was identified according to the m/z ratio and the retention time, determined from a separate chromatogram with pure acetyl-CoA only. The results were normalized according to the internal standards and the cell number, and the relative quantification is expressed as arbitrary unit.

In situ hybridization

In situ hybridization (ISH) was performed as described previously (*56*). Templates were amplified by PCR from oligo-dT–primed cDNA prepared from total RNA of fetal human neocortical tissue using the following primers (forward: 5’-

TAATTGAGAGCCAGATACAGACCA-3'; reverse: 5'-GCTTCATACACAGTAATTCCAGCT-3'), and an antisense RNA probe directed against the TKTL1 mRNA was synthesized using the DIG RNA labeling Mix (Roche). ISH was performed on 20 µm- and 40 µm-thick cryosections of PCW 11 fetal human frontal and occipital neocortical tissue as well as 20 µm-thick cryosections of day 50 cerebral organoids. Prior to the hybridization step, cryosections were sequentially treated with 0.2 M HCl (2x 5 min, room temperature) and then with 5 µg/ml proteinase K in PBS, pH 7.4 (10 min, room temperature). Hybridization was performed overnight at 65˚C with 20 ng/ml of the antisense RNA probe. The signal was detected immunohistochemically with anti-digoxigenin-AP antibody (Roche, #11093274910, RRID:AB_2734716) and NBT/BCIP (Roche, #11681451001) as color substrate.

TKTL1 expression analysis by RT-qPCR

TKTL1 gene expression analysis by RT-qPCR was performed as previously described (*57*). Total RNA was isolated from PCW 9, 11, 12, 13 and 15 human neocortical tissue, and from PCW 11, 16 and 17 human neocortical frontal and occipital lobe tissue, using the RNeasy Mini Kit (Qiagen) according to the manufacturer's instructions. cDNA synthesis was performed using the Maxima first-strand cDNA synthesis kit for RT-qPCR (Thermo Scientific). A LightCycler® 96 Instrument (Roche) and the FastStart essential DNA green master (Roche) were used to carry out the qPCR. Gene expression data were normalized based on the housekeeping gene GAPDH. The following primers were used: GAPDH: forward: 5'-TGAAGCAGGCATCTGAGGG, reverse: 5'-CGAAGGTGGAAGAGTGGGAG; TKTL1 ENST00000369912.2: forward: 5'-GCTGGGAGAAATGACCGCTT, reverse: 5'-TGATGTAGGGTGGCTGAAAGA; TKTL1 ENST00000369912.2 and ENST00000369915.8: forward: 5'-AAGCCAATGCCGAGAGAAAG, reverse: 5'-CTGTAATCAGGTGGAGAGGT.

Quantification

All quantifications were performed using Fiji. Cells were quantified in standardized microscopic fields, as indicated in the figures. All quantifications were done blindly. Any pVim+ cell located ≥30 µm away from the apical surface of the VZ was counted as BP.

For the analyses of BP and bRG morphotypes in P2 ferret brains, we used previously described criteria (*31*). Briefly, BPs were identified as PCNA+ cells in the iSVZ and oSVZ, and their morphology was classified in 6 different morphotypes (multipolar BPs, bRG with a basal process, bRG with an apical process, bRG with apical and basal processes, bRG with bifurcated basal process, and bRG with apical and bifurcated basal processes) based on the FP+ staining.

For the P16 ferret brains, the morphological measures were performed, as previously described (*44*), at two positions along the rostro-caudal axis. Briefly, the dorsal neocortex lateral length, the gyrus size and the local gyrification index are presented as a ratio of the value of the electroporated hemisphere (IUE) over the value of the contralateral non-electroporated hemisphere (non-IUE). The lateral length of the dorsal neocortex and of the electroporated area were determined as depicted in Figure 6I and Figure S6B, respectively. The local gyrification index was determined as the ratio of the length of the inner contour over the length of the outer contour (Fig. S6D). The gyrus size was determined for the gyrus that was located in the center of the electroporated area and for the corresponding gyrus on the contralateral side.

As the number of dead cells, determined using DAPI staining, did not vary significantly between mock-edited (hTKTL1) and gene-edited (aTKTL1) cerebral organoids (Fig. S8G), the dead cells were excluded from the quantification of the various cell types in these organoids.

Statistical analyses

Sample sizes (biological replicates) used for statistical tests are reported in each figure legend. Mouse embryos and fetal human tissue samples were randomly selected for the various experimental conditions. Mouse, human tissue, and cerebral organoid samples were excluded from further analyses only if the samples appeared to be severely damaged or dead, or if the electroporation efficiency was clearly lower than normal or was not comparable between the different groups of samples. No predetermination of sample sizes was carried out because our research is an exploratory study. The sample sizes are listed in the figure legends. Each experiment was independently performed at least 3 times. Data were processed with Excel (Microsoft) and analyzed with Prism (GraphPad Software). The normality of distribution was tested using either the Kolmogorov-Smirnov or the Shapiro-Wilk test, and the equality of variance was confirmed using the F-test. Parametric statistical tests were used for normally distributed samples, and non-parametric statistical tests for non-normally distributed samples. The parametric tests used were two-tailed unpaired or paired Student's t-test, one-way analysis of variance (ANOVA) followed by Tukey's multiple comparison tests, or two-way ANOVA followed by Bonferroni's post-hoc test. The non-parametric tests used were Mann Whitney U-test, Kruskal-Wallis test followed by Dunn's multiple comparison test or Friedman test followed by Dunn's multiple comparison test.

Fig. S1

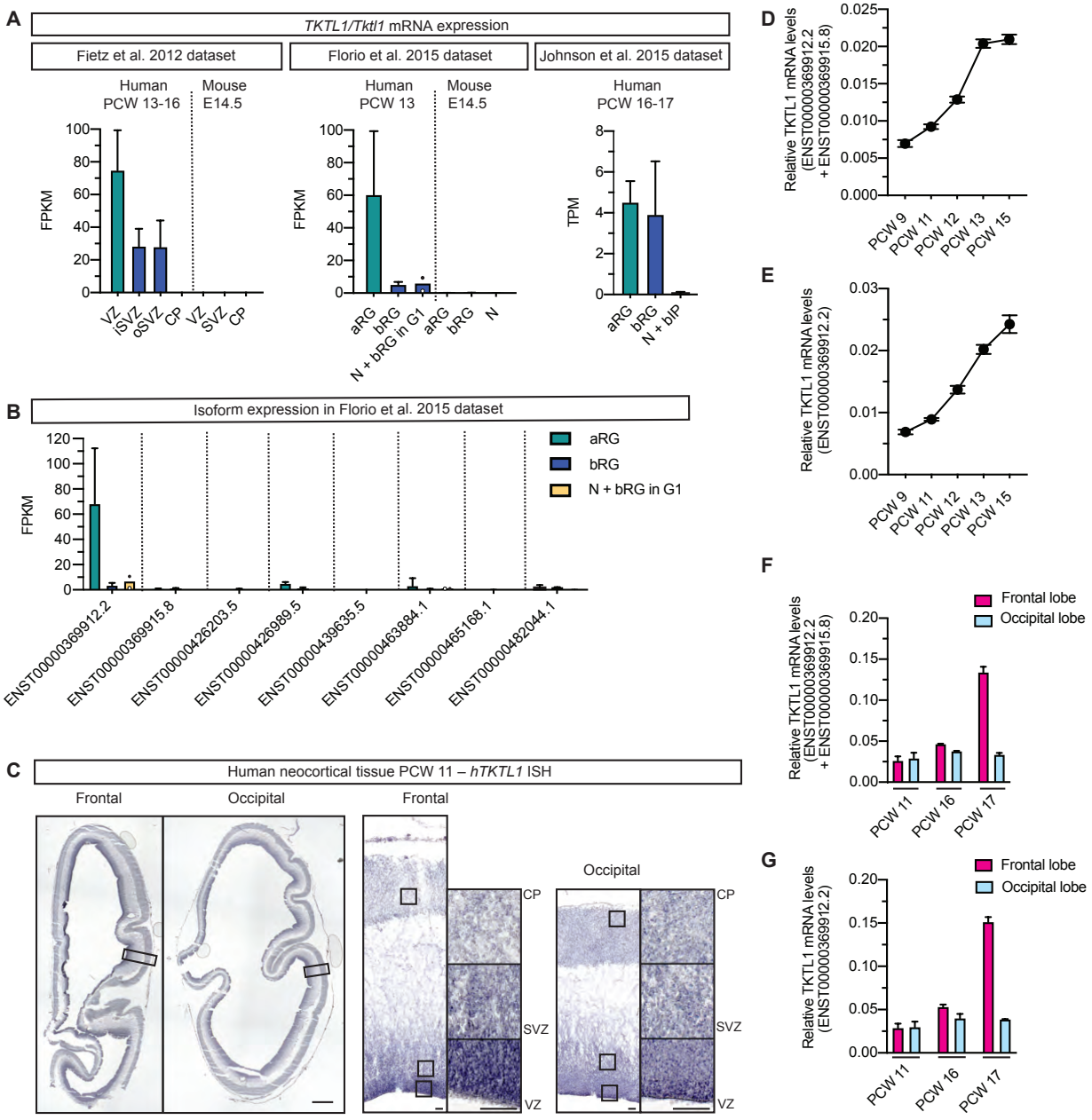

H

```
  1 MADAEARAEFPEEARPDRGTLQVLQDMASRLRIHSIRATCSTSSGHPTSC
  1  51 SSSSEIMSVLFFYIMRYKQSDPENPDNDRFVLAKRLSFVDVATGWLGQGL
 45 101 GVACGMAYTGKYFDRASYRVFCLMSDGESSEGSVWEAMAFASYYSLDNLV
 95 151 AIFDVNRLGHSGALPAEHCINIYQRRCEAFGWNTYVVDGRDVEALCQVFW
145 201 QASQVKHKPTAVVAKTFKGRGTPSIEDAESWHAKPMPRERADAIIKLIES
195 251 QIQTSRNLDPQPPIEDSPEVNITDVRMTSPPDYRVGDKIATRKACGLALA
245 301 KLGYANNRVVVLDGDTRYSTFSEIFNKEYPERFIECFMAEQNMVSVALGC
295 351 ASRGRTIAFASTFAAFLTRAFDHIRIGGLAESNINIIGSHCGVSVGDDGA
345 401 SQMALEDIAMFRTIPKCTIFYPTDAVSTEHAVALAANAKGMCFIRTTRPE
395 451 TMVIYTPQERFEIGQAKVLRHCVSDKVTVIGAGITVYEALAAADELSKQD
445 501 IFIRVIDLFTIKPLDVATIVSSAKATEGRIITVEDHYPQGGIGEAVCAAV
495 551 SMDPDIQVHSLAVSGVPQSGKSEELLDMYGISARHIIVAVKCMLLN
```

Fig. S1. Analysis of *TKTL1* mRNA levels in fetal human neocortex reveals highest expression in the frontal lobe.

(**A**) Left: Mean FPKM values of *TKTL1* mRNA expression in the indicated neocortical zones of fetal human neocortical tissue (six PCW 13-16 fetuses) and embryonic mouse neocortex (five E14.5 embryos) {Fietz, 2012 #13014}. Error bars, SD. Middle: Mean FPKM values of *TKTL1* mRNA expression in the indicated isolated cell populations (N, neurons) of (i) PCW 13 fetal human neocortical tissue (aRG and bRG, 4 samples, 2 different fetal samples, each subjected to 2 independent cell isolations; N + bRG in G1, 2 samples, 2 different fetal samples, 1 cell isolation each) and (ii) embryonic mouse neocortex (four E14.5 embryos) {Florio, 2015 #12451}. Error bars, SD; for N + bRG in G1, the two dots indicate the individual values. Right: Mean TPM values of *TKTL1* mRNA expression in the indicated isolated cell population of three PCW 16-17 fetal human neocortical tissues {Johnson, 2015 #12684}. Error bars, SD.

(**B**) Mean *TKTL1* mRNA splice variant expression in the indicated isolated cell populations (N, neurons) of PCW 13 fetal human neocortical tissue assessed using the Kallisto algorithm {Florio, 2018 #13812} and the data reported in {Florio, 2015 #12451}. The splice variants are indicated by Ensembl transcript IDs. For sample numbers and error bars, see (A).

(**C**) In situ hybridization analysis of *TKTL1* mRNA expression in the fetal human neocortex using a specific antisense probe. Left: Coronal sections of the frontal and occipital lobes of the neocortex at PCW 11. Scale bar, 1 mm. Right: Higher magnification of the cortical wall in the positions of the frontal and occipital lobes as indicated by the boxes on the left. The three boxed areas in each image indicate areas of the VZ, SVZ and CP that are shown at even higher magnification on the right. Scale bars, 50 μm.

(**D, E**) RT-qPCR analysis of the expression of the sum of the short (ENST00000369912.2) plus long (ENST00000369915.8) *TKTL1* isoforms (D), or of only the short (ENST00000369912.2) *TKTL1* isoform (E), in fetal human neocortical tissue at the indicated developmental stages (PCW 9-15). The level of *TKTL1* expression is expressed relative to that of the housekeeping gene *GAPDH*. Mean of 3 technical replicates from one fetus at each developmental stage. Error bars, SD.

(**F, G**) RT-qPCR analysis of the expression of the sum of the short (ENST00000369912.2) plus long (ENST00000369915.8) *TKTL1* isoforms (F), or of only the short (ENST00000369912.2) *TKTL1* isoform (G), in fetal human neocortical frontal vs. occipital lobe tissue at the indicated developmental stages (PCW 11-17). The level of *TKTL1* expression is expressed relative to that of the housekeeping gene *GAPDH*. Mean of 3 technical replicates from one fetus at each developmental stage. Error bars, SD.

(**H**) Amino acid sequence of the long (grey plus black letters) and short (black letters only) TKTL1 isoforms. The arginine317 in the long isoform, corresponding to arginine261 in the short isoform (red), is the modern human-specific amino acid residue that is a lysine in the Neandertal {Prüfer, 2014 #12447} and Denisovan {Meyer, 2012 #12448} sequence. The numbers of the first amino acid of each row of the long isoform (blue numbers) and the short isoform (green numbers) are indicated on the left.

Fig. S2

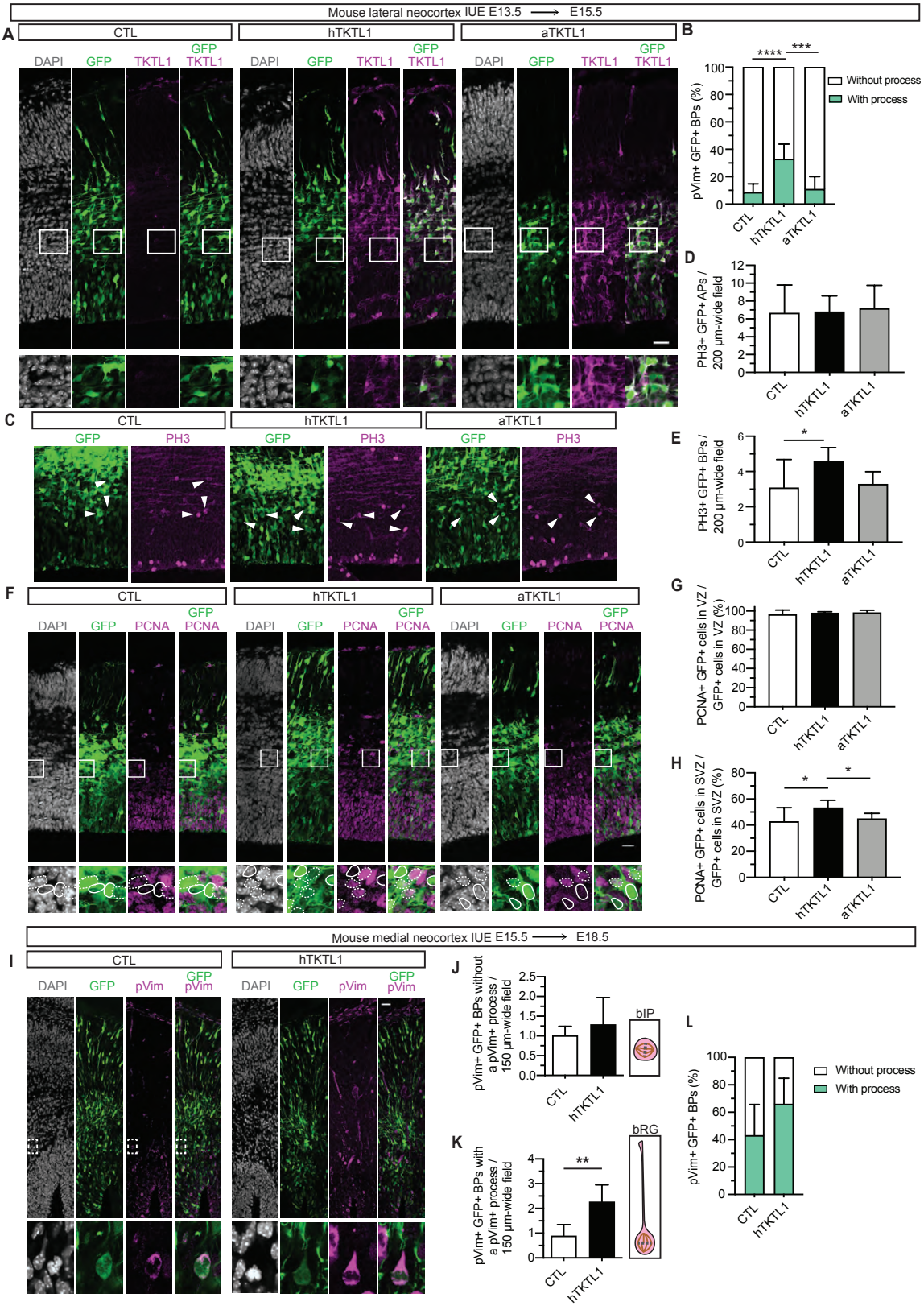
Mouse lateral neocortex IUE E13.5 ⟶ E15.5
A
CTL
hTKTL1
aTKTL1
DAPI
GFP
TKTL1
GFP TKTL1
B
pVim+ GFP+ BPs (%)
Without process
With process
****
***
C
GFP
PH3
D
PH3+ GFP+ APs / 200 µm-wide field
E
PH3+ GFP+ BPs / 200 µm-wide field
F
PCNA
GFP PCNA
G
PCNA+ GFP+ cells in VZ / GFP+ cells in VZ (%)
H
PCNA+ GFP+ cells in SVZ / GFP+ cells in SVZ (%)
Mouse medial neocortex IUE E15.5 ⟶ E18.5
I
pVim
GFP pVim
J
pVim+ GFP+ BPs without a pVim+ process / 150 µm-wide field
bIP
K
pVim+ GFP+ BPs with a pVim+ process / 150 µm-wide field
bRG
L
pVim+ GFP+ BPs (%)
CTL
hTKTL1
aTKTL1

Fig. S2. Modern human TKTL1, but not archaic TKTL1, when expressed in embryonic mouse lateral and medial neocortex, increases proliferating BPs and the proportion of bRG among BPs.

(**A-H**) Mouse lateral neocortex was electroporated *in utero* (IUE) at E13.5 with a pCAGGS plasmid encoding GFP, together with either an empty pCAGGS plasmid (control, CTL), a plasmid encoding modern human TKTL1 (hTKTL1), or a plasmid encoding archaic TKTL1 (aTKTL1) as indicated, followed by analyses at E15.5.

(**A**) Immunofluorescence of cryosections of CTL– (left), hTKTL1– (middle) and aTKTL1– (right) electroporated E15.5 lateral neocortex for GFP (green) and TKTL1 (magenta) combined with DAPI staining (grey). White dashed boxed areas are shown at higher magnification below the respective images. Scale bar, 30 μm.

(**B**) Percentages of pVim+ GFP+ mitotic BPs without (mitotic bIPs, white) vs. with (mitotic bRG, green) a pVim+ process. Means of 8 embryos. Error bars, SD. One-way ANOVA with Tukey post-hoc test, **** $p < 0.0001$, *** $p < 0.001$.

(**C**) Immunofluorescence of cryosections of CTL– (left), hTKTL1– (middle) and aTKTL1– (right) electroporated E15.5 lateral neocortex for GFP (green) and PH3 (magenta). Arrowheads indicate GFP+ PH3+ BPs. Scale bar, 30 μm.

(**D, E**) Quantification of PH3+ GFP+ mitotic APs (D) and BPs (E) in a 200-μm wide field. Means of 8 embryos. Error bars, SD. (D) One-way ANOVA, not significant; (E) one-way ANOVA with Tukey post-hoc test, * $p < 0.05$.

(**F**) Immunofluorescence of cryosections of CTL– (left), hTKTL1– (middle) and aTKTL1– (right) electroporated E15.5 lateral neocortex for GFP (green) and PCNA (magenta) combined with DAPI staining (grey). White boxed areas are shown at higher magnification below the respective images. White dashed lines indicate GFP+ PCNA+ BP nuclei, white solid lines GFP+ PCNA– BP nuclei. Scale bar, 25 μm.

(**G, H**) Percentages of GFP+ cells in VZ (G) and SVZ (H) that are PCNA+. Means of 7 to 10 embryos. Error bars, SD. (G) One-way ANOVA, not significant; (H) one-way ANOVA with Tukey post-hoc test, * $p < 0.05$.

(**I-L**) Mouse medial neocortex was electroporated *in utero* (IUE) at E15.5 with a pCAGGS plasmid encoding GFP, together with either an empty pCAGGS vector (control, CTL) or a plasmid encoding modern human TKTL1 (hTKTL1), followed by analyses at E18.5.

(**I**) Immunofluorescence of cryosections of CTL– (left) and hTKTL1– (right) electroporated E18.5 medial neocortex for GFP (green) and pVim (magenta) combined with DAPI staining (grey). The white dashed boxed area in the SVZ is shown at higher magnification below the CTL images and shows a GFP+ pVim+ BP without a pVim+ process (mitotic bIP). The white solid boxed area in the SVZ is shown at higher magnification below the hTKTL1 images and shows a GFP+ pVim+ BP with a pVim+ basal process (mitotic bRG). Scale bar, 30 μm.

(**J, K**) Quantification of pVim+ GFP+ mitotic BPs without a pVim+ process (J, bIPs, as illustrated) and with a pVim+ process (K, bRG, as illustrated) in a 150-μm wide field. Means of 6 embryos. Error bars, SD. Student's *t*-test, (J) not significant, (K) ** $p < 0.01$.

(**L**) Percentages of pVim+ GFP+ mitotic BPs without (mitotic bIPs, white) vs. with (mitotic bRG, green) a pVim+ process. Means of 6 embryos. Error bars, SD. Student's *t*-test, not significant.

Fig. S3

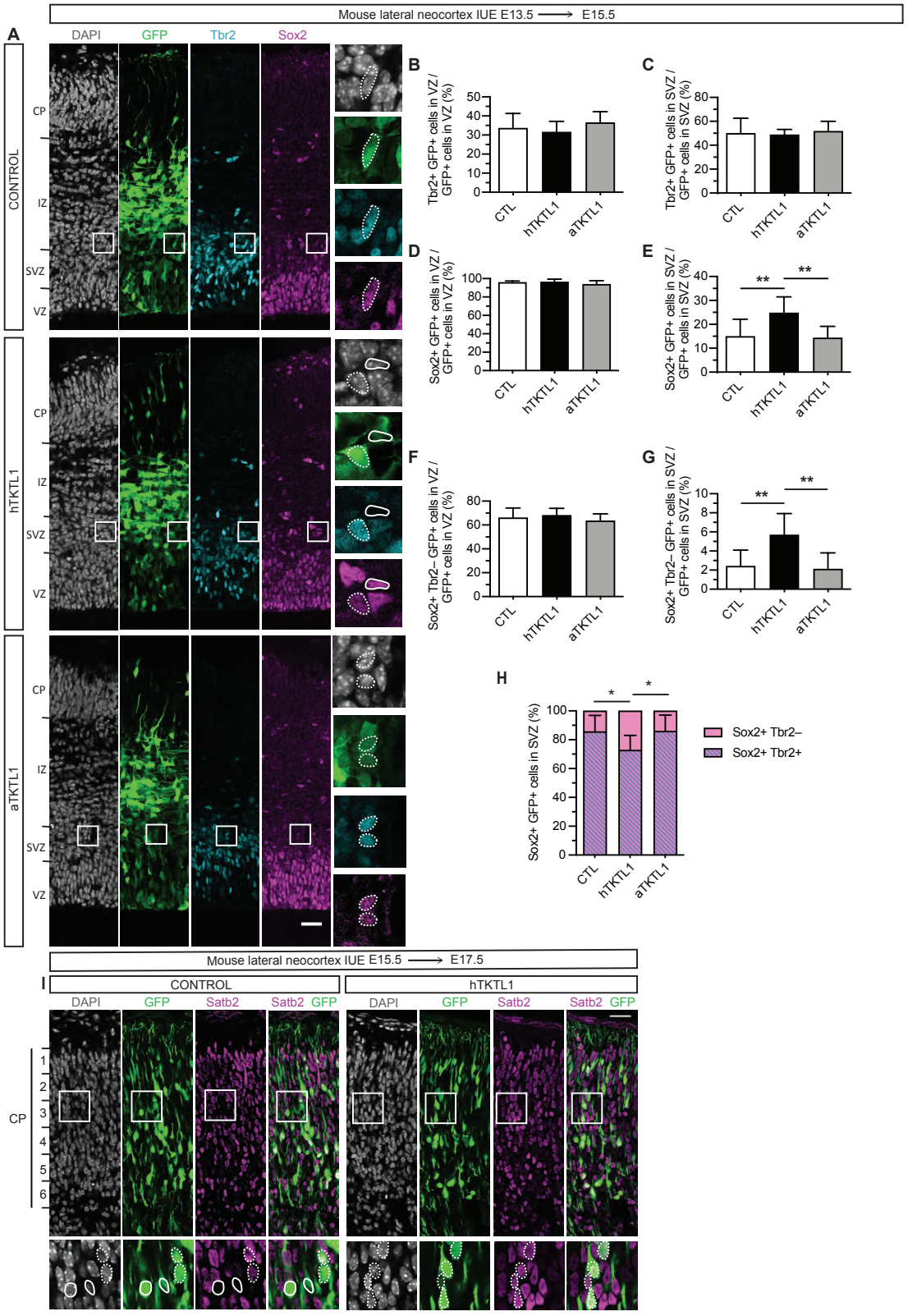
Mouse lateral neocortex IUE E13.5 ⟶ E15.5
A
DAPI
GFP
Tbr2
Sox2
CONTROL
hTKTL1
aTKTL1
CP
IZ
SVZ
VZ
B
Tbr2+ GFP+ cells in VZ / GFP+ cells in VZ (%)
C
Tbr2+ GFP+ cells in SVZ / GFP+ cells in SVZ (%)
D
Sox2+ GFP+ cells in VZ / GFP+ cells in VZ (%)
E
Sox2+ GFP+ cells in SVZ / GFP+ cells in SVZ (%)
F
Sox2+ Tbr2– GFP+ cells in VZ / GFP+ cells in VZ (%)
G
Sox2+ Tbr2– GFP+ cells in SVZ / GFP+ cells in SVZ (%)
CTL
hTKTL1
aTKTL1
H
Sox2+ GFP+ cells in SVZ (%)
Sox2+ Tbr2–
Sox2+ Tbr2+
Mouse lateral neocortex IUE E15.5 ⟶ E17.5
I
CONTROL
hTKTL1
DAPI
GFP
Satb2
Satb2 GFP
CP
1
2
3
4
5
6

Fig. S3. Modern human TKTL1, but not archaic TKTL1, when expressed in embryonic mouse lateral neocortex, increases Sox2+ BPs.
(**A-H**) Mouse lateral neocortex was electroporated *in utero* (IUE) at E13.5 with a pCAGGS plasmid encoding GFP, together with either an empty pCAGGS plasmid (control, CTL), a plasmid encoding modern human TKTL1 (hTKTL1), or a plasmid encoding archaic TKTL1 (aTKTL1), followed by analyses at E15.5.
(**A**) Immunofluorescence of cryosections of control– (top), hTKTL1– (middle) and aTKTL1– (bottom) electroporated E15.5 lateral neocortex for GFP (green), Tbr2 (cyan), Sox2 (magenta) combined with DAPI staining (grey). White boxed areas in the SVZ are shown at higher magnification on the right. White dashed lines indicate GFP+ Tbr2+ Sox2+ nuclei. White solid line indicates a GFP+ Sox2+ but Tbr2– nucleus. Scale bar, 30 μm.
(**B-H**) Quantifications in E15.5 lateral neocortex. Means of 9 embryos. Error bars, SD.
(**B, C**) Percentage of GFP+ cells in VZ (B) and SVZ (C) that are Tbr2+. One-way ANOVA, not significant.
(**D, E**) Percentage of GFP+ cells in VZ (D) and SVZ (E) that are Sox2+. (D) One-way ANOVA, not significant; (E) one-way ANOVA with Tukey post-hoc test, ** $p < 0.01$.
(**F, G**) Percentage of GFP+ cells in the VZ (F) and SVZ (G) that are Sox2+ Tbr2–. (F) Kruskal-Wallis test, not significant; (G) one-way ANOVA with Tukey post-hoc test, ** $p < 0.01$.
(**H**) Percentages of Sox2+ GFP+ cells in SVZ that are either Tbr2+ or Tbr2–. One-way ANOVA with Tukey post-hoc test, * $p < 0.05$.
(**I**) Mouse lateral neocortex was electroporated *in utero* (IUE) at E13.5 with a pCAGGS plasmid encoding GFP, together with either an empty pCAGGS plasmid (control, CTL) or a plasmid encoding modern human TKTL1 (hTKTL1), followed by analyses at E17.5. Immunofluorescence of cryosections of control– (left) and hTKTL1– (right) electroporated E17.5 neocortex for GFP (green) and Satb2 (magenta) combined with DAPI (grey) staining. White boxed areas in the CP are shown at higher magnification below the respective images. White dashed lines indicate GFP+ Satb2+ nuclei, white solid lines GFP+ Satb2– nuclei. Scale bar, 30 μm.

Fig.S4

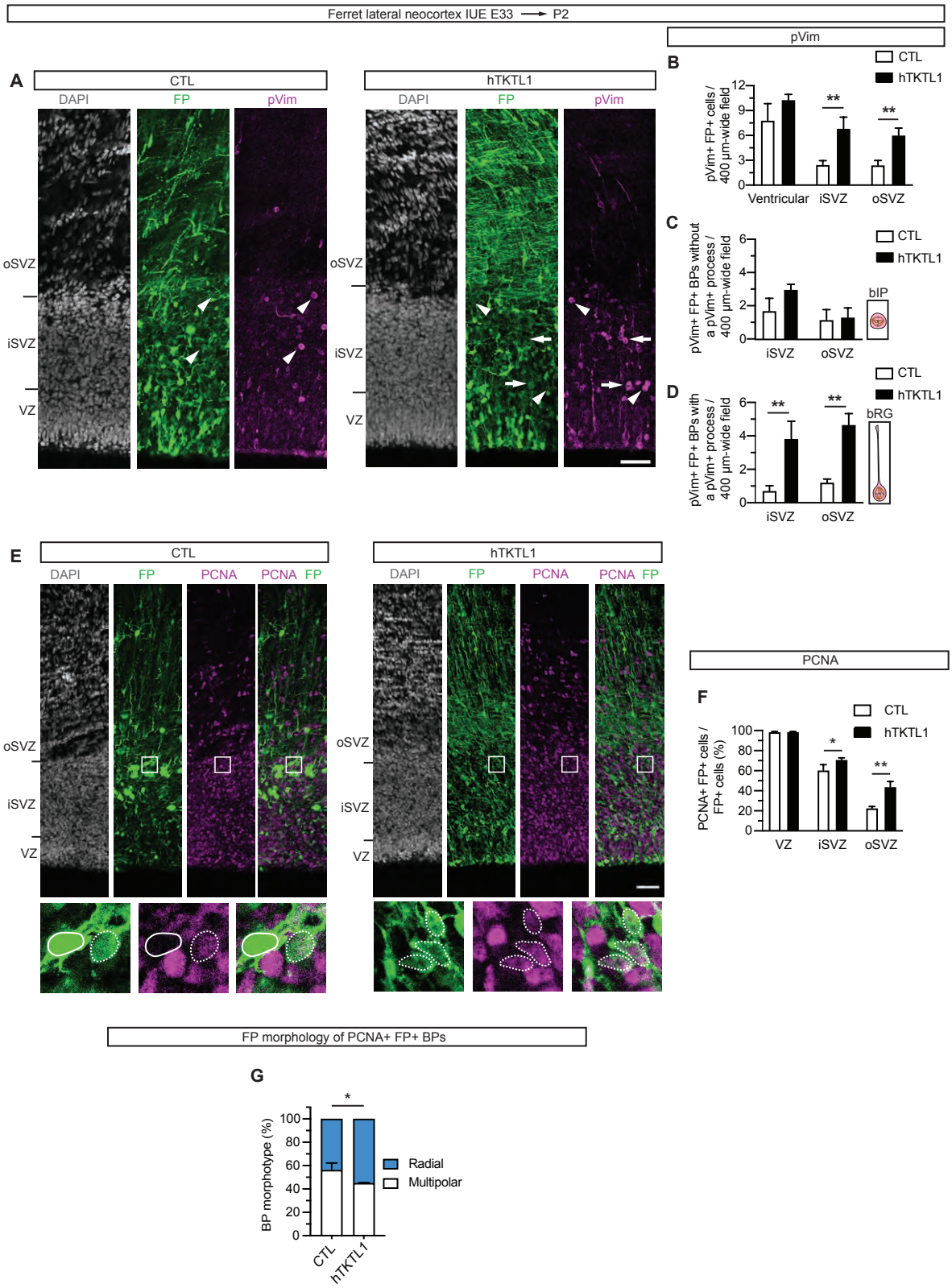
Ferret lateral neocortex IUE E33 → P2
A
CTL
hTKTL1
DAPI
FP
pVim
oSVZ
iSVZ
VZ
pVim
B
CTL
hTKTL1
pVim+ FP+ cells / 400 µm-wide field
Ventricular
iSVZ
oSVZ
C
pVim+ FP+ BPs without a pVim+ process / 400 µm-wide field
bIP
D
pVim+ FP+ BPs with a pVim+ process / 400 µm-wide field
bRG
E
PCNA
PCNA FP
PCNA
F
PCNA+ FP+ cells / FP+ cells (%)
FP morphology of PCNA+ FP+ BPs
G
BP morphotype (%)
Radial
Multipolar

Fig. S4. Modern human TKTL1, when expressed in developing ferret lateral neocortex, increases bRG abundance.

Ferret lateral neocortex was electroporated *in utero* (IUE) at E33 with a pCAGGS plasmid encoding either GFP or mCherry (collectively referred to as fluorescent protein, FP; see Methods), together with either an empty pCAGGS plasmid (control, CTL) or a plasmid encoding modern human TKTL1 (hTKTL1), followed by analyses at P2.

(**A**) Immunofluorescence of cryosections of CTL– (left) and hTKTL1– (right) electroporated P2 lateral neocortex for FP (green) and pVim (magenta) combined with DAPI staining (grey). Arrowheads indicate FP+ pVim+ BPs without a pVim+ process (mitotic bIPs). Arrows indicate FP+ pVim+ BPs with a pVim+ process (mitotic bRG). Scale bar, 50 μm.

(**B**-**D**) Quantifications in 400 μm-wide fields of P2 lateral neocortex. Means of 3 embryos. Error bars, SD.

(**B**) Total pVim+ FP+ cells located at the ventricular surface of the VZ and in the iSVZ and oSVZ. Student's *t*-test, ** $p < 0.01$.

(**C**) pVim+, FP+ mitotic BPs without a pVim+ process (mitotic bIPs, as illustrated) located in the iSVZ and oSVZ. Student's *t*-test, not significant.

(**D**) pVim+, FP+ mitotic BPs with a pVim+ process (mitotic bRG, as illustrated) located in the iSVZ and oSVZ. Student's *t*-test, ** $p < 0.01$.

(**E**) Immunofluorescence of cryosections of CTL– (left) and hTKTL1– (right) electroporated P2 lateral neocortex for FP (green) and PCNA (magenta) combined with DAPI staining (grey). White boxed areas are shown at higher magnification below the corresponding images. White dashed lines indicate PCNA+ FP+ nuclei, white solid line indicate a PCNA– FP+ nucleus. Scale bar, 50 μm.

(**F-H**) Quantifications in P2 lateral neocortex. Means of 3 embryos. Error bars, SD.

(**F**) Percentages of the FP+ cells in the VZ, iSVZ and oSVZ that are PCNA+. Student's *t*-test, * $p < 0.05$, ** $p < 0.01$.

(**G**) Percentages of PCNA+ cells in SVZ (BPs) that have multipolar vs. radial morphology. Student's *t*-test, * $p < 0.05$.

(**H**) Percentages of PCNA+ radial cells in SVZ (bRG) that exhibit one of the 5 morphotypes illustrated on the right. Two-way ANOVA with Bonferroni post-hoc test, * $p < 0.05$, ** $p < 0.01$.

Fig. S5

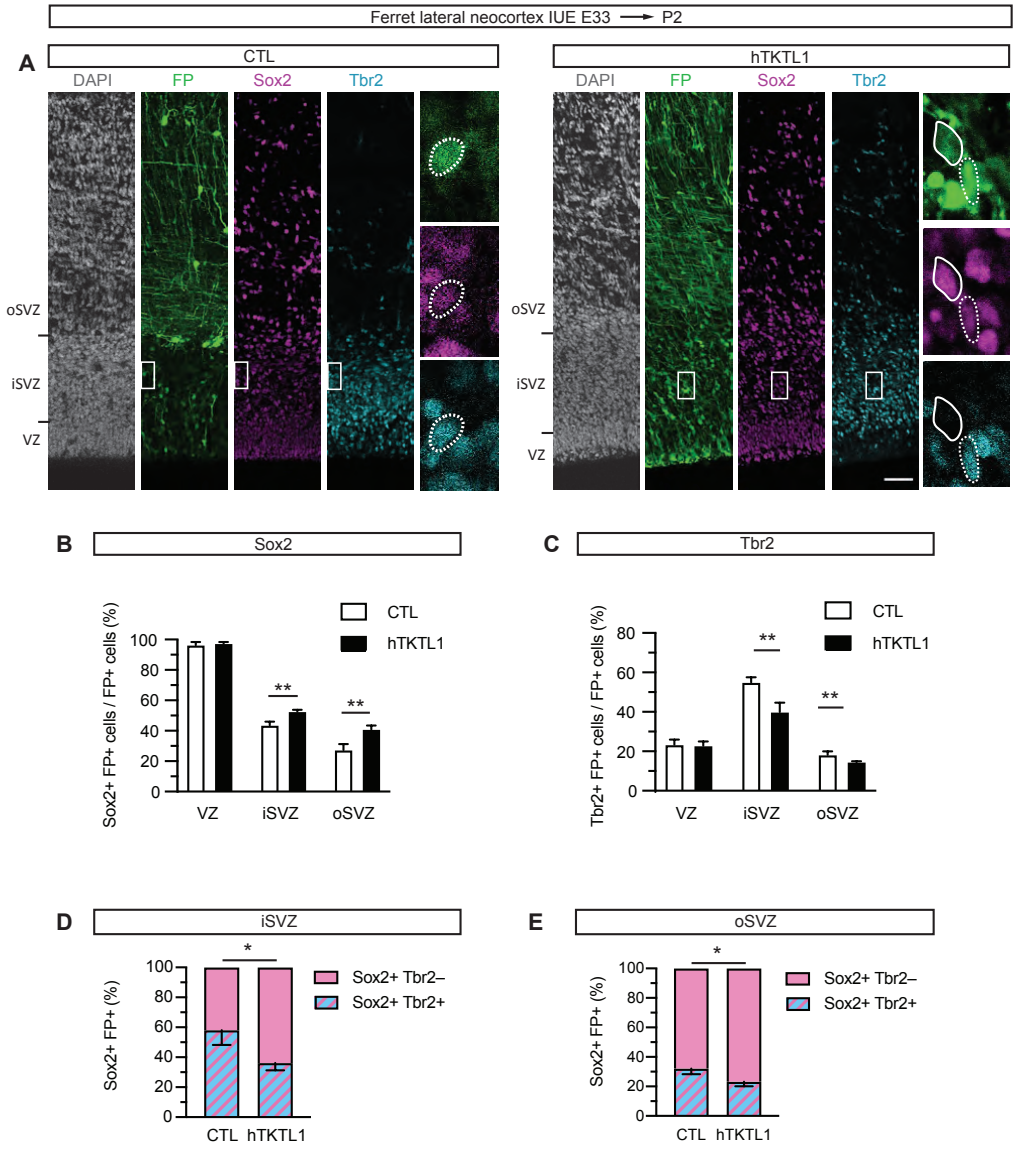
Ferret lateral neocortex IUE E33 → P2
A
CTL
hTKTL1
DAPI
FP
Sox2
Tbr2
oSVZ
iSVZ
VZ
B
Sox2
Sox2+ FP+ cells / FP+ cells (%)
CTL
hTKTL1
VZ
iSVZ
oSVZ
C
Tbr2
Tbr2+ FP+ cells / FP+ cells (%)
D
iSVZ
Sox2+ FP+ (%)
Sox2+ Tbr2–
Sox2+ Tbr2+
CTL
hTKTL1
E
oSVZ

Fig. S5. Modern human TKTL1, when expressed in developing ferret lateral neocortex, increases Sox2+ BPs.

Ferret lateral neocortex was electroporated *in utero* (IUE) at E33 with a pCAGGS plasmid encoding either GFP or mCherry (collectively referred to as fluorescent protein, FP; see Methods), together with either an empty pCAGGS plasmid (control, CTL) or a plasmid encoding modern human TKTL1 (hTKTL1), followed by analyses at P2.

(**A**) Immunofluorescence of cryosections of CTL– (left) and hTKTL1– (right) electroporated P2 lateral neocortex for FP (green), Sox2 (magenta) and Tbr2 (cyan) combined with DAPI staining (grey). White boxed areas in the iSVZ are shown at higher magnification on the right. White dashed lines indicate Sox2+ Tbr2+ FP+ nuclei, white solid line indicates a Sox2+ Tbr2– FP+ nucleus. Scale bar, 50 μm.

(**B-E**) Quantifications in P2 lateral neocortex. Means of 3 embryos. Error bars, SD.

(**B, C**) Percentages of the FP+ cells in the VZ, iSVZ and oSVZ that are Sox2+ (B) and Tbr2+ (C). Student's *t*-test, ** $p < 0.01$.

(**D, E**) Percentages of the Sox2+ FP+ cells in the iSVZ (L) and oSVZ (M) that are either Tbr2+ (blue with magenta stripes) or Tbr2– (magenta). Student's *t*-test, * $p < 0.05$.

Fig. S6

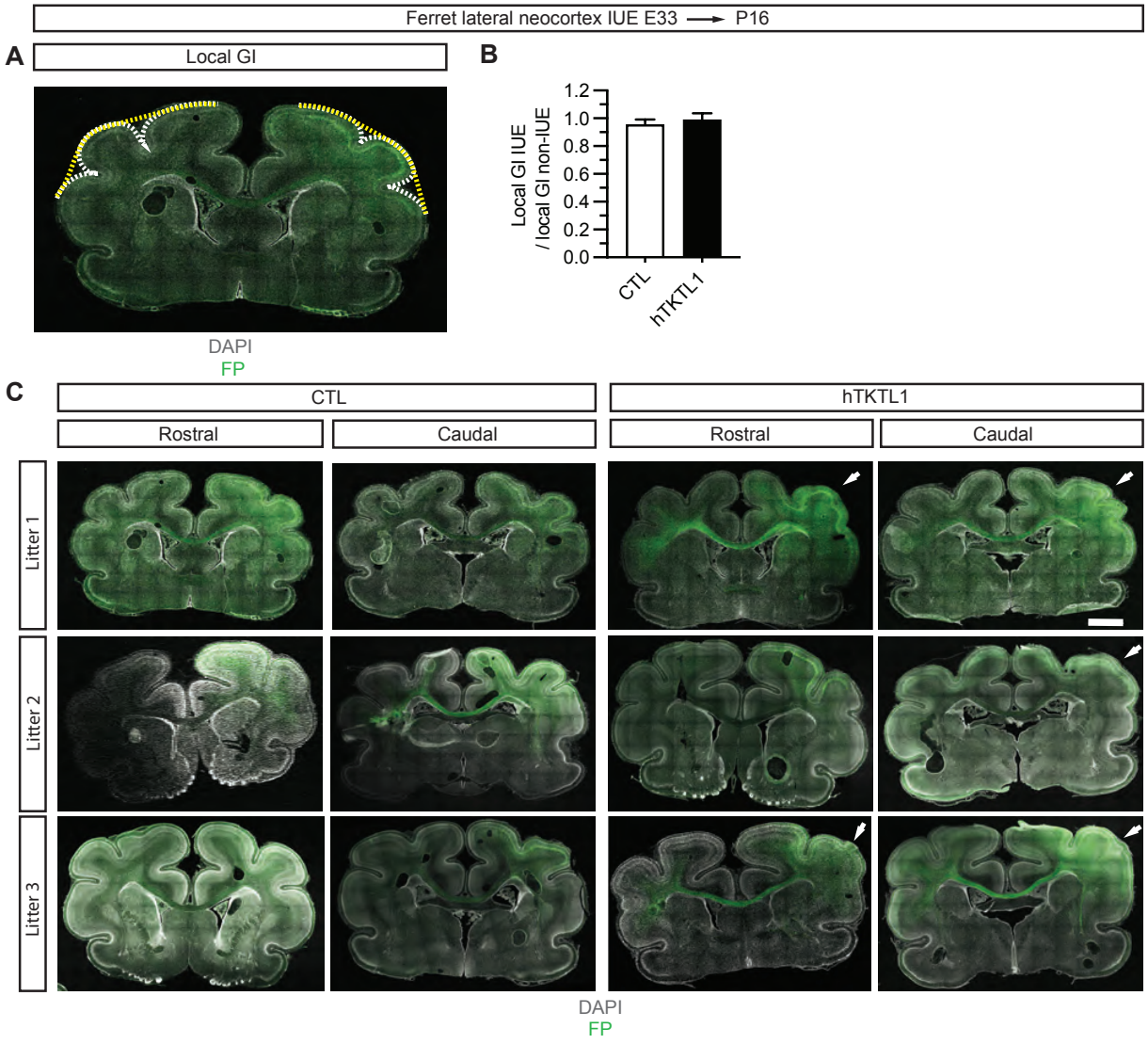
Ferret lateral neocortex IUE E33 → P16
A
Local GI
DAPI
FP
B
Local GI IUE / local GI non-IUE
1.2
1.0
0.8
0.6
0.4
0.2
0.0
CTL
hTKTL1
C
CTL
hTKTL1
Rostral
Caudal
Rostral
Caudal
Litter 1
Litter 2
Litter 3
DAPI
FP

Fig. S6. Modern human TKTL1, when expressed in developing ferret lateral neocortex, increases folding in half of the neocortices without affecting local GI.
Ferret lateral neocortex was electroporated *in utero* (IUE) at E33 with a pCAGGS plasmid encoding either GFP or mCherry (collectively referred to as fluorescent protein, FP; see Methods), together with either an empty pCAGGS plasmid (control, CTL) or a plasmid encoding modern human TKTL1 (hTKTL1), followed by analyses at P16.
(**A**) Immunofluorescence of a cryosection of CTL–electroporated ferret P16 lateral neocortex for FP (green) combined with DAPI staining (grey). The local gyrification index (GI) is defined as the ratio of the actual surface of the folded neocortex over a hypothetical smooth surface, as illustrated by the white dashed line and the yellow dashed line, respectively.
(**B**) Local GI of CTL– and hTKTL1–electroporated ferret P16 lateral neocortex, expressed as the ratio of the electroporated (IUE) hemisphere (mean GI CTL 1.297, mean GI hTKTL1 1.359) over the contralateral (non-IUE) hemisphere (mean GI CTL 1.3673, mean GI hTKTL1 1.378). Means of 6 embryos. Error bars, SD. Student's *t*-test.
(**C**) Immunofluorescence of rostral and caudal cryosections of 3 CTL– (left) and 3 hTKTL1– (right) electroporated ferret P16 lateral neocortices each for FP (green) combined with DAPI staining (grey). Arrows indicate additional folding of the electroporated hemisphere. Scale bar, 1 mm.

Fig. S7

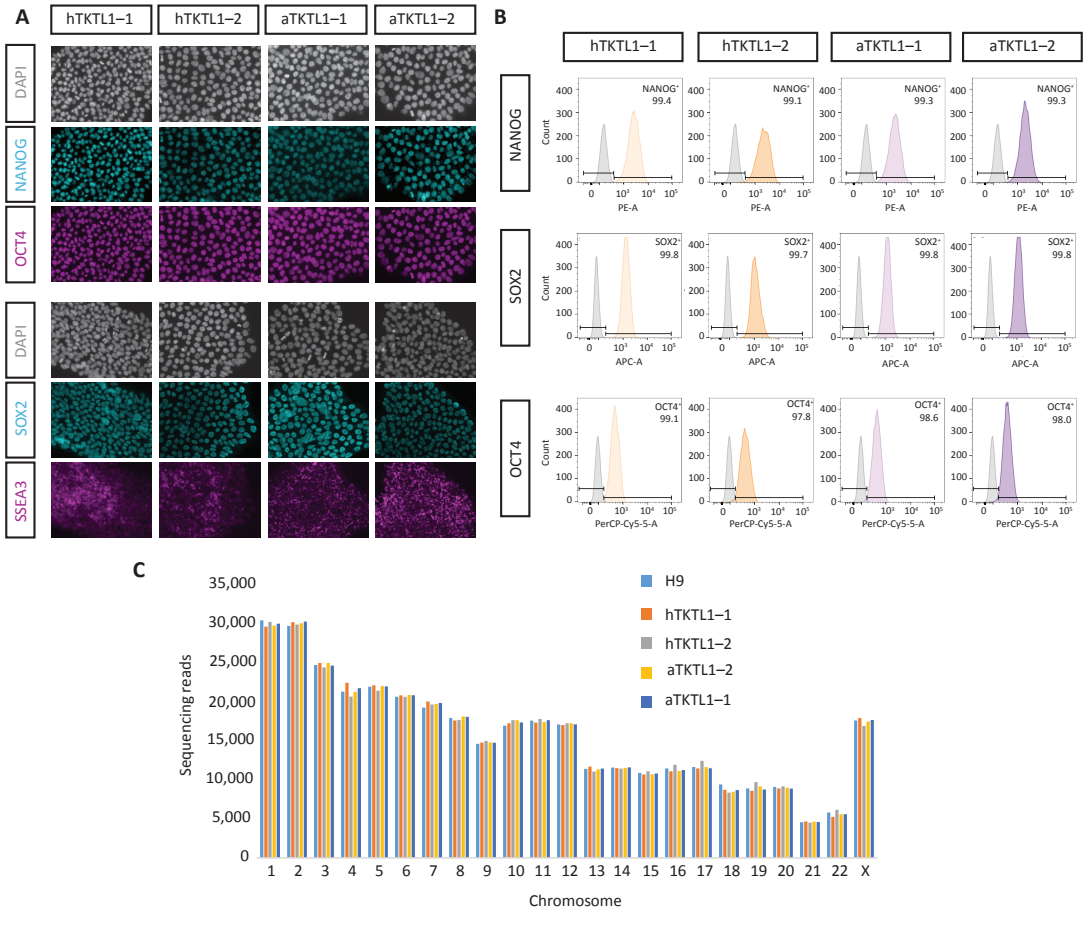
A
hTKTL1–1
hTKTL1–2
aTKTL1–1
aTKTL1–2
DAPI
NANOG
OCT4
DAPI
SOX2
SSEA3
B
hTKTL1–1
hTKTL1–2
aTKTL1–1
aTKTL1–2
NANOG
SOX2
OCT4
Count
PE-A
APC-A
PerCP-Cy5-5-A
NANOG+ 99.4
NANOG+ 99.1
NANOG+ 99.3
NANOG+ 99.3
SOX2+ 99.8
SOX2+ 99.7
SOX2+ 99.8
SOX2+ 99.8
OCT4+ 99.1
OCT4+ 97.8
OCT4+ 98.6
OCT4+ 98.0
C
H9
hTKTL1–1
hTKTL1–2
aTKTL1–2
aTKTL1–1
Sequencing reads
35,000
30,000
25,000
20,000
15,000
10,000
5,000
0
1 2 3 4 5 6 7 8 9 10 11 12 13 14 15 16 17 18 19 20 21 22 X
Chromosome
D
hTKTL1–1
aTKTL1–1
hTKTL1–2
aTKTL1–2

Fig. S7. H9 Human ESCs genome-edited to express archaic TKTL1 show no change in pluripotency and karyotype.
Two mock-edited H9 human ESC clones (hTKTL1–1, hTKTL1–2) and two *aTKTL1*-edited H9 human ESC clones (aTKTL1–1, aTKTL1–2), were analyzed for expression of pluripotency markers (A, B), by shallow DNA sequencing to detect any chromosomal aneuploidies and large-scale chromosomal duplications and deletions as compared to the mother H9 line (C), and for karyotype (D).
(**A**) Immunofluorescence of mock-edited and *aTKTL1*-edited H9 human ESCs for either NANOG (cyan) and OCT4 (magenta) combined with DAPI staining (grey) (top three rows), or SOX2 (cyan) and stage-specific embryonic antigen 3, SSEA3 (magenta), combined with DAPI staining (grey) (bottom three rows).
(**B**) Flow cytometry analysis of mock-edited and *aTKTL1*-edited H9 human ESCs stained for NANOG, OCT4 and SOX2. The percentage of cells expressing a given marker is indicated in the top right corner. Grey curves: cells stained with isotype control antibody. Light and dark orange curves: immunostained mock-edited H9 ESCs. Light and dark purple curves: immunostained *aTKTL1*-edited H9 ESCs.
(**C**) Number of reads mapping to each chromosome in H9 human ESCs used for genome editing (light blue); hTKTL1–1 (orange) and hTKTL1–2 (grey) mock-edited H9 human ESCs; aTKTL1–1 (dark blue) and aTKTL1–2 (yellow) *aTKTL1*-edited H9 human ESCs. Sequencing reads were downsampled to match the number of reads in the cell line with lowest sequencing coverage.
(**D**) Karyograms of the two mock-edited and the two *aTKTL1*-edited H9 human ESCs. The karyotypes of the hTKTL1–1, hTKTL1–2, aTKTL1–1 and aTKTL1–2 cells are identical.

Fig. S8

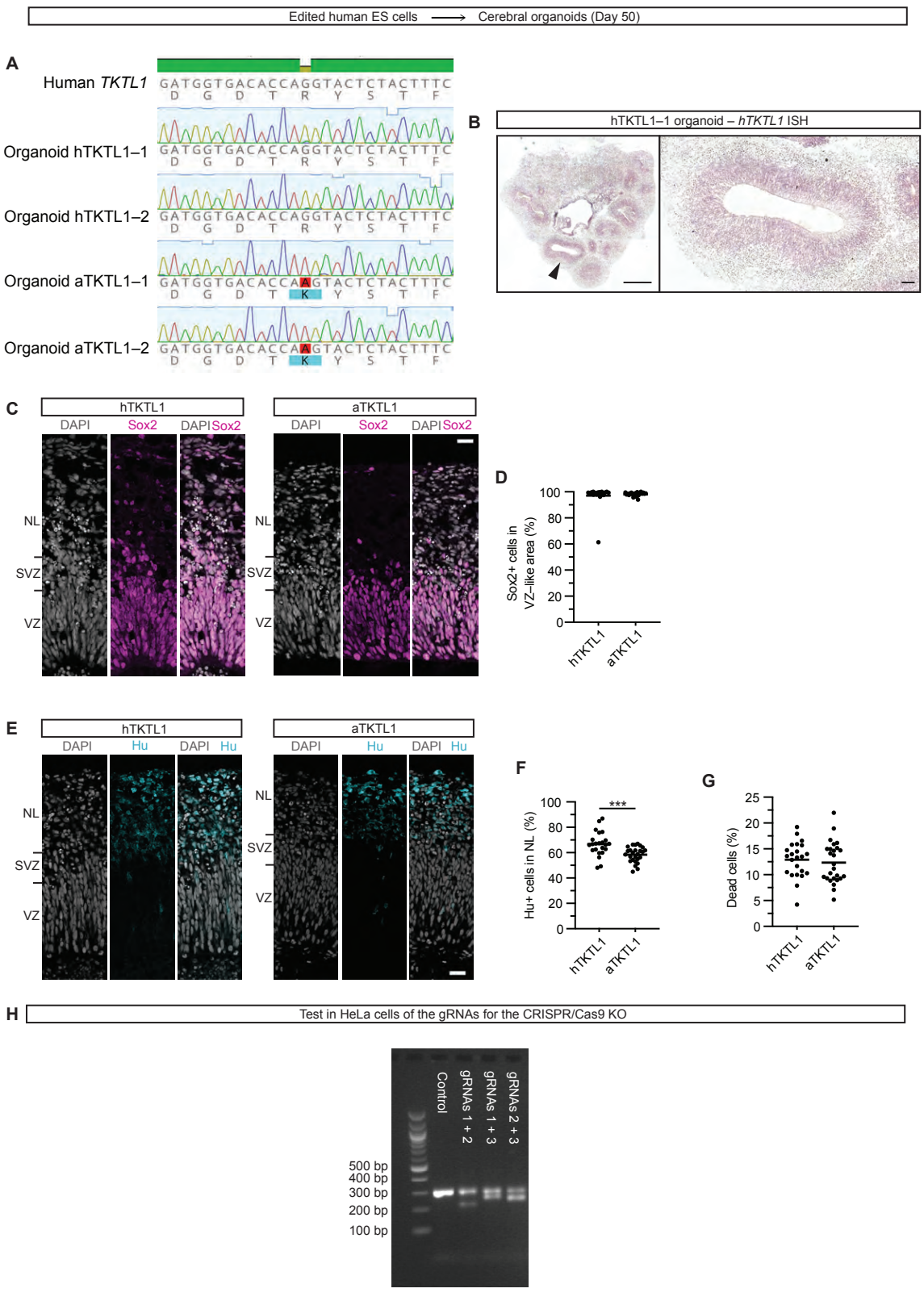
Edited human ES cells ⟶ Cerebral organoids (Day 50)
A
Human TKTL1
Organoid hTKTL1–1
Organoid hTKTL1–2
Organoid aTKTL1–1
Organoid aTKTL1–2
B
hTKTL1–1 organoid – hTKTL1 ISH
C
hTKTL1
aTKTL1
DAPI
Sox2
NL
SVZ
VZ
D
Sox2+ cells in VZ-like area (%)
hTKTL1
aTKTL1
E
Hu
F
Hu+ cells in NL (%)
***
G
Dead cells (%)
H
Test in HeLa cells of the gRNAs for the CRISPR/Cas9 KO
Control
gRNAs 1 + 2
gRNAs 1 + 3
gRNAs 2 + 3
500 bp
400 bp
300 bp
200 bp
100 bp

Fig. S8. Human cerebral organoids, derived from ESCs genome-edited to express archaic TKTL1, exhibit a reduction in Hu+ neurons.
(**A**) *TKTL1* DNA and deduced amino acid sequences in 50 day-old cerebral organoids grown from two mock-edited human ESC clones (hTKTL1-1, hTKTL1-2) and two *TKTL1*-edited human ESC clones (aTKTL1-1, aTKTL1-2), aligned with the corresponding segment of the human *TKTL1* sequence.
(**B**) Coronal sections of 50 day-old human cerebral organoids (hTKTL1-1) were subjected to in situ hybridization (ISH) using a specific antisense probe to detect *TKTL1* mRNA expression. The arrowhead indicates a ventricle-like structure shown at higher magnification on the right. Scale bars, left 500 µm, right 50 µm.
(**C**) Immunofluorescence of cryosections of modern human (hTKTL1-2, left) and archaic (aTKTL1-1, right) TKTL1-expressing human cerebral organoids for Sox2 (magenta) combined with DAPI staining (grey). Scale bar, 25 µm.
(**D**) Percentages of the cells in the VZ-like area that are Sox2+ in hTKTL1 and aTKTL1 human cerebral organoids. Means of 21 hTKTL1 (9 hTKTL1-1, 12 hTKTL1-2) and 23 aTKTL1 (12 aTKTL1-1, 11 aTKTL1-2) organoids. Mann-Whitney U-test, not significant,.
(**E**) Immunofluorescence of cryosections of modern human (hTKTL1-2, left) and archaic (aTKTL1-1, right) human cerebral organoids for Hu (cyan) combined with DAPI staining (grey). Scale bar, 25 µm.
(**F**) Percentage of the cells in neuronal layer that are Hu+ in hTKTL1 and aTKTL1 human cerebral organoids. Means of 23 hTKTL1 (9 hTKTL1-1, 14 hTKTL1-2) and 26 aTKTL1 (12 aTKTL1-1, 14 aTKTL1-2) organoids. Student's *t*-test, *** $p < 0.001$.
(**G**) Percentage of dead cells determined using DAPI-staining. Means of 23 hTKTL1– (9 hTKTL1-1, 14 hTKTL1-2) and 26 aTKTL1– (12 aTKTL1-1, 14 aTKTL1-2) organoids. Unpaired Student's *t*-test, not significant.
(**H**) Electrophoresis gel showing the efficiency of the 3 different pairs of gRNAs to induce Cas9-mediated cutting of the *hTKTL1* gene in HeLa cells. HeLa cells were either mock-electroporated (Control) or electroporated with *in vitro* prepared complexes of recombinant Cas9 protein and the indicated gRNAs targeting *hTKTL1*, followed by PCR analysis of the targeted region of the *hTKTL1* gene. The pair of gRNAs 2 and 3 was chosen for the *hTKTL1* KO in fetal human neocortical tissue.

Fig. S9

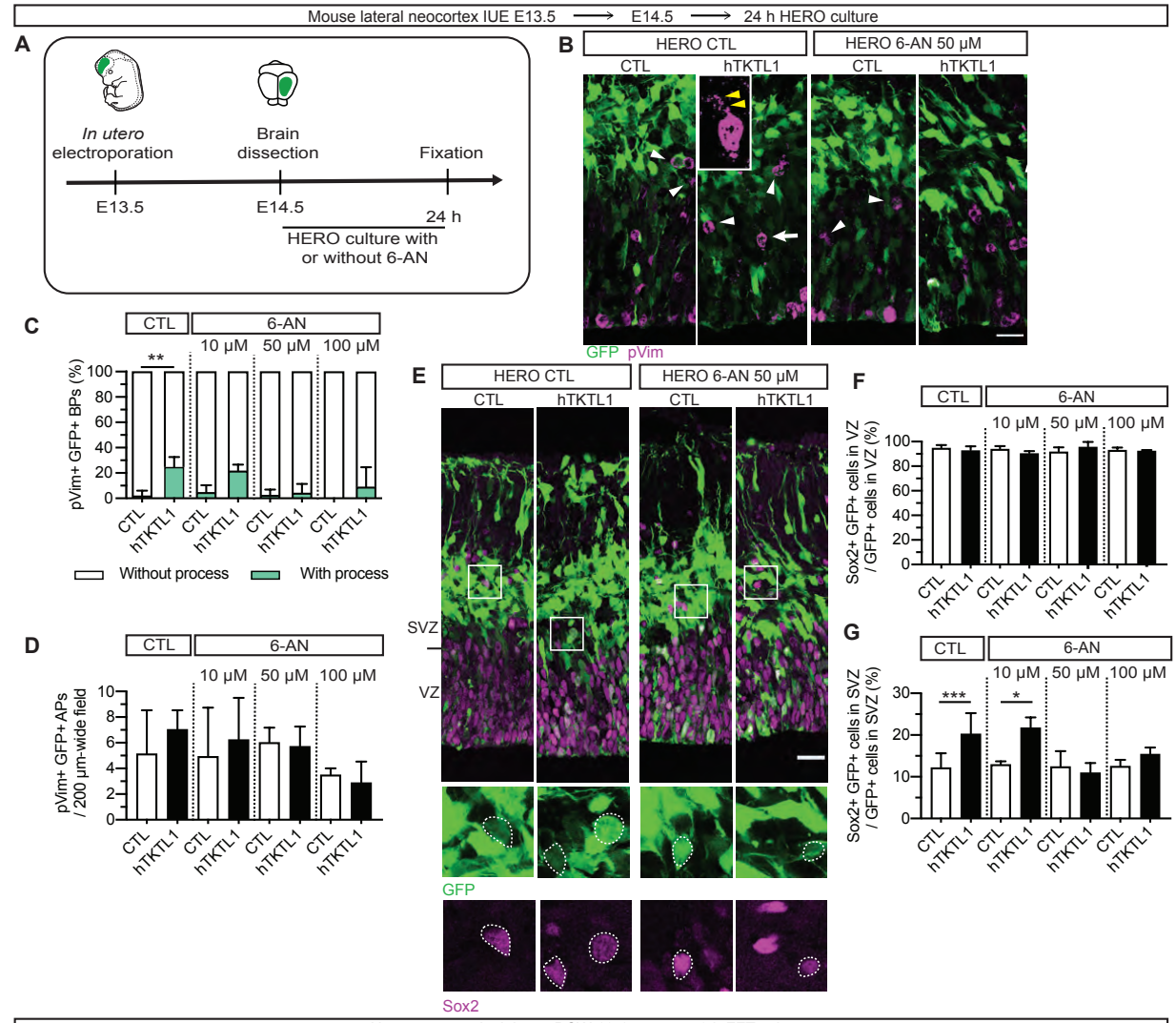
Mouse lateral neocortex IUE E13.5 ⟶ E14.5 ⟶ 24 h HERO culture
A
In utero electroporation
Brain dissection
Fixation
E13.5
E14.5
24 h
HERO culture with or without 6-AN
B
HERO CTL
HERO 6-AN 50 µM
CTL
hTKTL1
GFP pVim
C
CTL
6-AN
10 µM 50 µM 100 µM
pVim+ GFP+ BPs (%)
Without process
With process
D
pVim+ GFP+ APs / 200 µm-wide field
E
SVZ
VZ
GFP
Sox2
F
Sox2+ GFP+ cells in VZ / GFP+ cells in VZ (%)
G
Sox2+ GFP+ cells in SVZ / GFP+ cells in SVZ (%)
Human neocortical tissue PCW 10-14 ⟶ 48 h FFT culture
H
6-AN 50 µM
DAPI Active caspase 3
I
Active caspase 3+ cells in VZ + SVZ / 200 µm-wide field

Fig. S9. Inhibition of the pentose phosphate pathway by 6-AN abolishes the hTKTL1-induced increase in Sox2+ GFP+ BPs and in the proportion of bRG among BPs in embryonic mouse lateral neocortex, and has no effect on apoptosis in fetal human neocortical tissue.
(**A**) Schematic representation of the experimental protocol of mouse hemisphere rotation (HERO) culture. Mouse lateral neocortex was electroporated at E13.5 with a pCAGGS plasmid encoding GFP, together with either an empty pCAGGS plasmid (control, CTL) or a plasmid encoding modern human TKTL1 (hTKTL1). The brain was dissected at E14.5 and the hemispheres were subjected to 24 hours of hemisphere rotation (HERO) culture in the absence (CTL) or presence of 10, 50 or 100 µM of 6-AN, followed by fixation and analyses.
(**B**) Immunofluorescence for GFP (green) and pVim (magenta) of cryosections of CTL– and hTKTL1–electroporated E14.5 mouse neocortex subjected to HERO culture for 24 hours without (CTL, left) or with (6-AN, right) 50 µM 6-AN. White arrowheads indicate GFP+ pVim+ BPs without a process (mitotic bIPs). The arrow indicates a GFP+ pVim+ BP with a pVim+ process (mitotic bRG), shown at higher magnification in the inset. Yellow arrowheads indicate the basal process. Scale bar, 25 µm.
(**C, D**) Quantifications after HERO culture as described in (A). Means of 3 to 9 embryos. Error bars, SD.
(**C**) Percentages of pVim+ GFP+ mitotic BPs without (mitotic bIPs, white) vs. with (mitotic bRG, green) a pVim+ process in CTL– and hTKTL1–electroporated neocortex cultured without (CTL) or with (6-AN) 10, 50 or 100 µM of 6-AN. Kruskal-Wallis with Dunn post-hoc test, ** $p < 0.01$.
(**D**) pVim+ GFP+ mitotic APs in a 200 µm-wide field of CTL– and hTKTL1–electroporated neocortex cultured without (CTL) or with (6-AN) 10, 50 or 100 µM of 6-AN. Two-way ANOVA, not significant.
(**E**) Immunofluorescence for GFP (green) and Sox2 (magenta) of cryosections of CTL– and hTKTL1–electroporated E14.5 mouse neocortex subjected to HERO culture for 24 hours without (CTL, left) or with (6-AN, right) 50 µM 6-AN. White boxed areas in the SVZ are shown at higher magnification below the respective images. The nuclei outlined by white dotted lines indicate Sox2+ GFP+ cells. Scale bar, 30 µm.
(**F, G**) Percentages of GFP+ cells in the VZ (F) and SVZ (G) that are Sox2+ in CTL– and hTKTL1–electroporated neocortex cultured without (CTL) or with (6-AN) 10, 50 or 100 µM of 6-AN. Means of 3 to 9 embryos. Error bars, SD. Two-way ANOVA (F, G) with Bonferroni post-hoc test (G), (F) not significant, (G) * $p < 0.05$, *** $p < 0.001$.
(**H**) Immunofluorescence of cryosections of PCW 10-14 fetal human neocortical tissue, subjected to free-floating tisse (FFT) culture for 48 hours without (control, CTL, left) or with (6-AN, right) 50 µM 6-AN, for active caspase 3 (magenta) combined with DAPI staining (grey). Arrowheads indicate active caspase 3+ cells. Scale bar, 30 µm.
(**I**) Quantification of active caspase 3+ cells in the VZ plus SVZ of a 200 µm-wide field of fetal human neocortical tissue subjected to FFT culture for 48 hours without (CTL) or with (6-AN) 10, 50 or 100 µM of 6-AN. Means of 3 to 5 different fetal samples, each of which is represented by a different color. One-way ANOVA, not significant.

Fig. S10

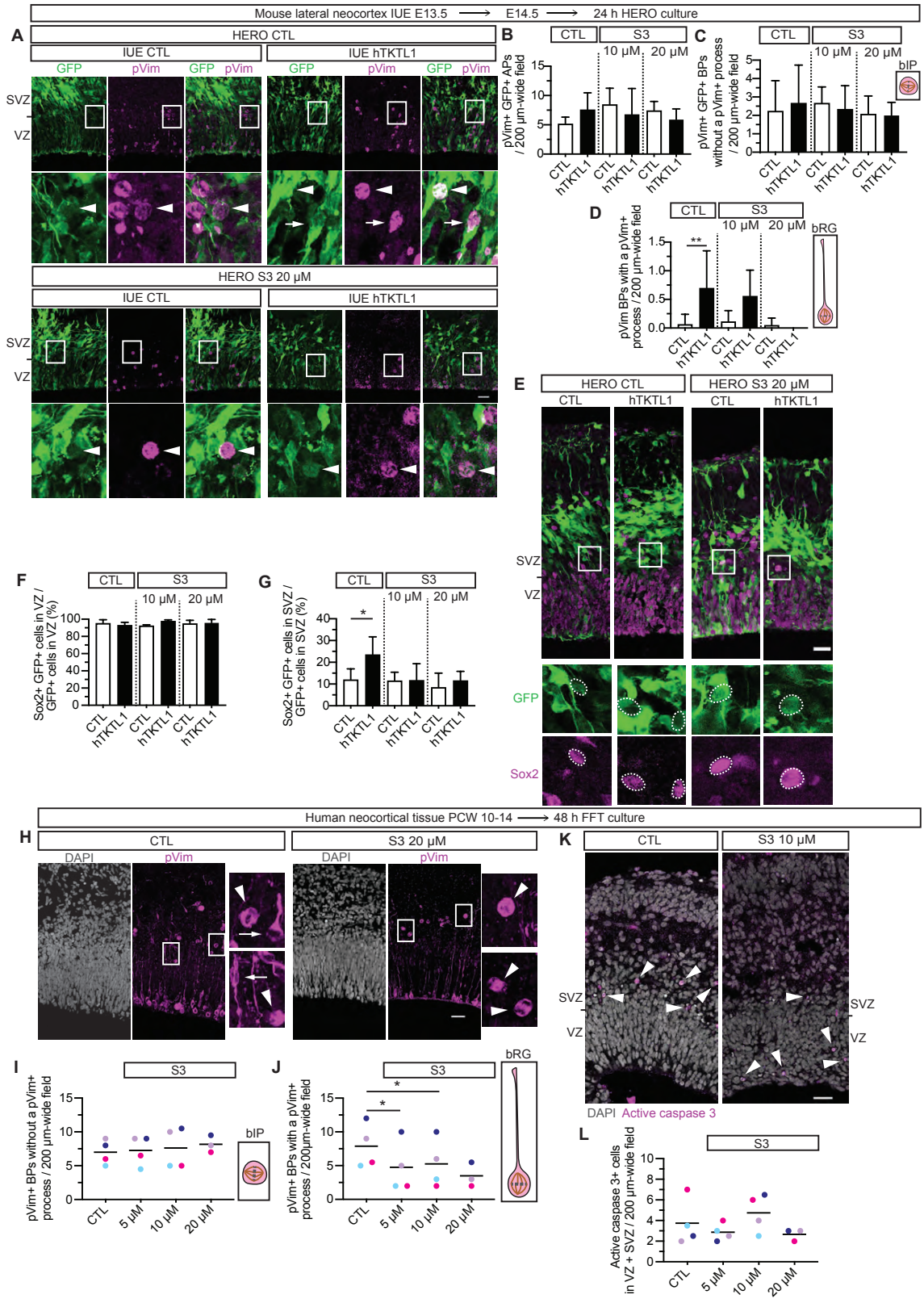
Mouse lateral neocortex IUE E13.5 ⟶ E14.5 ⟶ 24 h HERO culture
A
HERO CTL
IUE CTL
IUE hTKTL1
GFP
pVim
SVZ
VZ
HERO S3 20 µM
B
CTL
S3
10 µM
20 µM
pVim+ GFP+ APs / 200 µm-wide field
C
pVim+ GFP+ BPs without a pVim+ process / 200 µm-wide field
bIP
D
pVim BPs with a pVim+ process / 200 µm-wide field
bRG
E
HERO CTL
HERO S3 20 µM
hTKTL1
Sox2
F
Sox2+ GFP+ cells in VZ / GFP+ cells in VZ (%)
G
Sox2+ GFP+ cells in SVZ / GFP+ cells in SVZ (%)
Human neocortical tissue PCW 10-14 ⟶ 48 h FFT culture
H
S3 20 µM
DAPI
I
pVim+ BPs without a pVim+ process / 200 µm-wide field
J
pVim+ BPs with a pVim+ process / 200µm-wide field
K
S3 10 µM
DAPI Active caspase 3
L
Active caspase 3+ cells in VZ + SVZ / 200 µm-wide field

Fig. S10. Inhibition of the pentose phosphate pathway by S3 abolishes the hTKTL1-induced increase in bRG in embryonic mouse lateral neocortex and reduces bRG abundance, without affecting apoptosis, in fetal human neocortical tissue.

(**A-G**) Mouse lateral neocortex was electroporated *in utero* (IUE) at E13.5 with a pCAGGS plasmid encoding GFP, together with either an empty pCAGGS plasmid (control, CTL) or a plasmid encoding modern human TKTL1 (hTKTL1). The brain was dissected at E14.5 and the hemispheres were subjected to 24 hours of hemisphere rotation (HERO) culture in the absence (CTL) or presence of 10 or 20 μM of S3, a 6-phophogluconate dehydrogenase inhibitor, followed by analyses.

(**A**) Immunofluorescence for GFP (green) and pVim (magenta) of cryosections of CTL– and hTKTL1–electroporated E14.5 mouse neocortex subjected to HERO culture for 24 hours without (CTL, top) or with (S3, bottom) 20 μM S3. White boxed areas are shown at higher magnification below the respective images. Arrowheads indicate GFP+ pVim+ BPs without a process (mitotic bIPs). Arrows indicate a GFP+ pVim+ BP with a pVim+ process (mitotic bRG). Scale bar, 30 μm.

(**B-D**) Quantifications of pVim+ GFP+ mitotic (i) APs (B), (ii) BPs without a pVim+ process (mitotic bIPs, as illustrated) (C) and (iii) BPs with a pVim+ process (mitotic bRG, as illustrated) (D), in a 200 μm-wide field. Means of 3 to 9 embryos. Error bars, SD. Two-way ANOVA (B-D) with Bonferroni post-hoc test (D), (B, C) not significant, (D) ** $p < 0.01$.

(**E**) Immunofluorescence for GFP (green) and Sox2 (magenta) of cryosections of CTL– and hTKTL1–electroporated E14.5 mouse neocortex subjected to HERO culture for 24 hours without (CTL, left) or with (S3, right) 20 μM S3. White boxed areas in the SVZ are shown at higher magnification below the respective images. White dashed lines indicate Sox2+ GFP+ nuclei. Scale bar, 25 μm.

(**F, G**) Percentages of GFP+ cells in the VZ (F) and SVZ (G) that are Sox2+. Means of 3 to 7 embryos. Error bars, SD. Two-way ANOVA (F, G) with Bonferroni post-hoc test (G), (F) not significant, (G) * $p < 0.05$.

(**H-L**) Human neocortical tissue (PCW 10-14) was subjected to free-floating tissue (FFT) culture for 48 hours without (CTL) or with (S3) 5, 10 or 20 μM of S3.

(**H**) Immunofluorescence of cryosections of PCW 10-14 fetal human neocortical tissue, subjected to FFT culture for 48 hours without (CTL, left) or with (S3, right) 20 μM S3, for pVim (magenta) combined with DAPI staining (grey). White boxed areas in the SVZ are shown at higher magnification on the right. Arrowheads indicate GFP+ pVim+ BPs without a process (mitotic bIPs).Arrows indicate GFP+ pVim+ BPs with a pVim+ process (mitotic bRG). Scale bar, 30 μm.

(**I, J**) Quantifications of pVim+ mitotic BPs without a pVim+ process (mitotic bIPs, as illustrated) (I) or with a pVim+ process (mitotic bRG, as illustrated) (J) in a 200 μm-wide field. Means of 3 to 4 different fetal samples, each of which is represented by a different color. One-way ANOVA (I, J) with Tukey post-hoc test (J), (I) not significant, (J) * $p < 0.05$ (J).

(**K**) Immunofluorescence of cryosections of PCW 10-14 fetal human neocortical tissue subjected to FFT culture for 48 hours without (CTL, left) or with (S3, right) 10 μM S3, for active caspase 3 (magenta) combined with DAPI staining (grey). Arrowheads indicate active caspase 3+ cells. Scale bar, 30 μm.

(**L**) Quantification of active caspase 3+ cells in the VZ plus SVZ of a 200 μm-wide field. Means of 3 to 4 different fetal samples, each of which is represented by a different color. One-way ANOVA, not significant.

Fig.S11

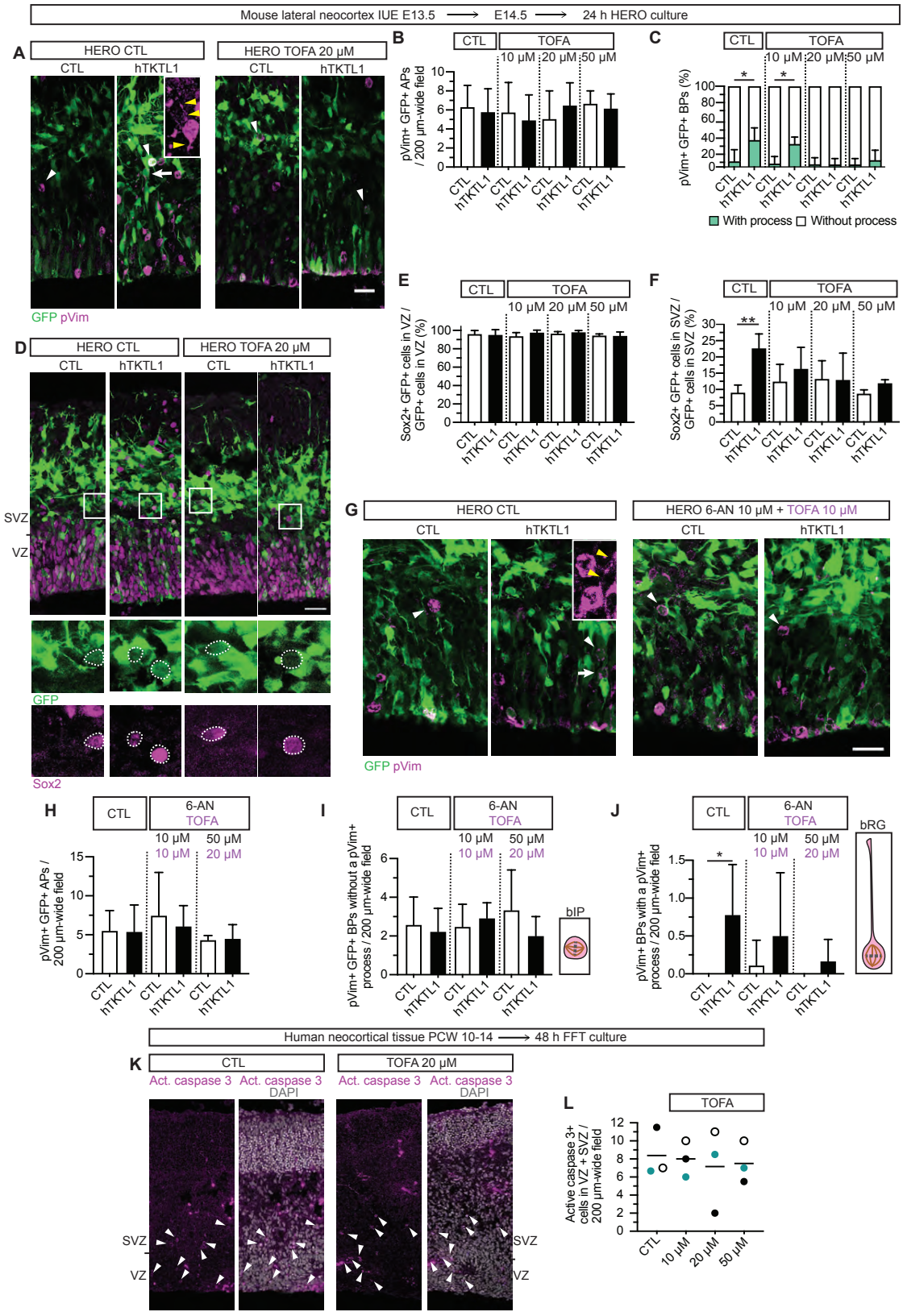
Mouse lateral neocortex IUE E13.5 ⟶ E14.5 ⟶ 24 h HERO culture
A
HERO CTL
HERO TOFA 20 µM
CTL
hTKTL1
GFP pVim
B
CTL
TOFA
10 µM 20 µM 50 µM
pVim+ GFP+ APs / 200 µm-wide field
C
pVim+ GFP+ BPs (%)
With process
Without process
D
SVZ
VZ
GFP
Sox2
E
Sox2+ GFP+ cells in VZ / GFP+ cells in VZ (%)
F
Sox2+ GFP+ cells in SVZ / GFP+ cells in SVZ (%)
G
HERO 6-AN 10 µM + TOFA 10 µM
H
6-AN
TOFA
10 µM 10 µM
50 µM 20 µM
I
pVim+ GFP+ BPs without a pVim+ process / 200 µm-wide field
bIP
J
pVim+ BPs with a pVim+ process / 200 µm-wide field
bRG
Human neocortical tissue PCW 10-14 ⟶ 48 h FFT culture
K
Act. caspase 3
DAPI
L
Active caspase 3+ cells in VZ + SVZ / 200 µm-wide field

Fig. S11. Inhibition of fatty acid synthesis by TOFA abolishes the hTKTL1-induced increase in Sox2+ GFP+ BPs and in the proportion of bRG among BPs in embryonic mouse lateral neocortex, and has no effect on apoptosis in fetal human neocortical tissue.

(**A-J**) Mouse lateral neocortex was electroporated *in utero* (IUE) at E13.5 with a pCAGGS plasmid encoding GFP, together with either an empty pCAGGS plasmid (control, CTL) or a plasmid encoding modern human TKTL1 (hTKTL1). The brain was dissected at E14.5 and the hemispheres were subjected to 24 hours of hemisphere rotation (HERO) culture in the absence (CTL) or presence of 10, 20 or 50 μM of TOFA (A-F) or in the absence (CTL) or presence of 10 μM 6-AN plus 10 μM TOFA or of 50 μM 6-AN plus 20 μM TOFA (G-J), followed by analyses.

(**A**) Immunofluorescence for GFP (green) and pVim (magenta) of cryosections of CTL– and hTKTL1–electroporated E14.5 mouse neocortex subjected to HERO culture for 24 hours without (CTL, left) or with (TOFA, right) 20 μM TOFA. Arrowheads indicate GFP+ pVim+ BPs without a pVim+ process (mitotic bIPs). Arrow indicates a GFP+ pVim+ BP with a pVim+ process (mitotic bRG), shown at higher magnification in the inset. Yellow arrowheads indicate the apical and basal processes. Scale bar, 25 μm.

(**B**) Quantification of pVim+ GFP+ mitotic APs in a 200 μm-wide field. Means of 5 to 7 embryos. Error bars, SD. Two-way ANOVA, not significant.

(**C**) Percentages of pVim+ GFP+ mitotic BPs without (mitotic bIPs, white) vs. with (mitotic bRG, green) a pVim+ process. Means of 5 to 7 embryos. Error bars, SD. Kruskal-Wallis with Dunn post-hoc test, * $p < 0.05$.

(**D**) Immunofluorescence for GFP (green) and Sox2 (magenta) of cryosections of CTL– and hTKTL1–electroporated E14.5 mouse neocortex subjected to HERO culture for 24 hours without (CTL, left) or with (TOFA, right) 20 μM TOFA. White boxed areas in the SVZ are shown at higher magnification below the respective images. White dashed lines indicate Sox2+ GFP+ nuclei. Scale bar, 30 μm.

(**E, F**) Percentages of GFP+ cells in the VZ (E) and SVZ (F) that are Sox2+. Means of 5 to 7 embryos. Error bars, SD. Two-way ANOVA (E, F) with Bonferroni post-hoc test (F), (E) not significant, (F) ** $p < 0.01$.

(**G**) Immunofluorescence for GFP (green) and pVim (magenta) of cryosections of CTL– and hTKTL1–electroporated E14.5 mouse neocortex subjected to HERO culture for 24 hours without (CTL, left) or with (6-AN + TOFA, right) 10 μM 6-AN plus 10 μM TOFA. Arrowheads indicate GFP+ pVim+ BPs without a pVim+ process (mitotic bIPs). Arrow indicates a GFP+ pVim+ BP with a pVim+ process (mitotic bRG), shown at higher magnification in the inset. Yellow arrowheads indicate the basal process. Scale bar, 25 μm.

(**H-J**) Quantifications of pVim+ GFP+ mitotic APs (H), BPs without a pVim+ process (mitotic bIPs, as illustrated) (I) and BPs with a pVim+ process (mitotic bRG, as illustrated) (J), in a 200-μm wide field. Means of 3 to 10 embryos. Error bars, SD. Two-way ANOVA (H-J) with Bonferroni post-hoc test (J), (H, I) not significant, (J) * $p < 0.05$.

(**K, L**) Human neocortical tissue (PCW 10-14) was subjected free-floating tissue (FFT) culture for 48 hours without (CTL) or with (TOFA) 10, 20 or 50 μM of TOFA.

(**K**) Immunofluorescence of cryosections of PCW 10-14 fetal human neocortical tissue, subjected to FFT culture for 48 hours without (CTL, left) or with (TOFA, right) 20 μM TOFA, for active caspase 3 (magenta) combined with DAPI staining (grey). Arrowheads indicate active caspase 3+ cells. Scale bar, 30 μm.

(L) Quantification of active caspase 3+ cells in the VZ plus SVZ of a 200 μm-wide field. Means of 3 different fetal samples, each of which is represented by a different color. One-way ANOVA, not significant.

Fig.S12

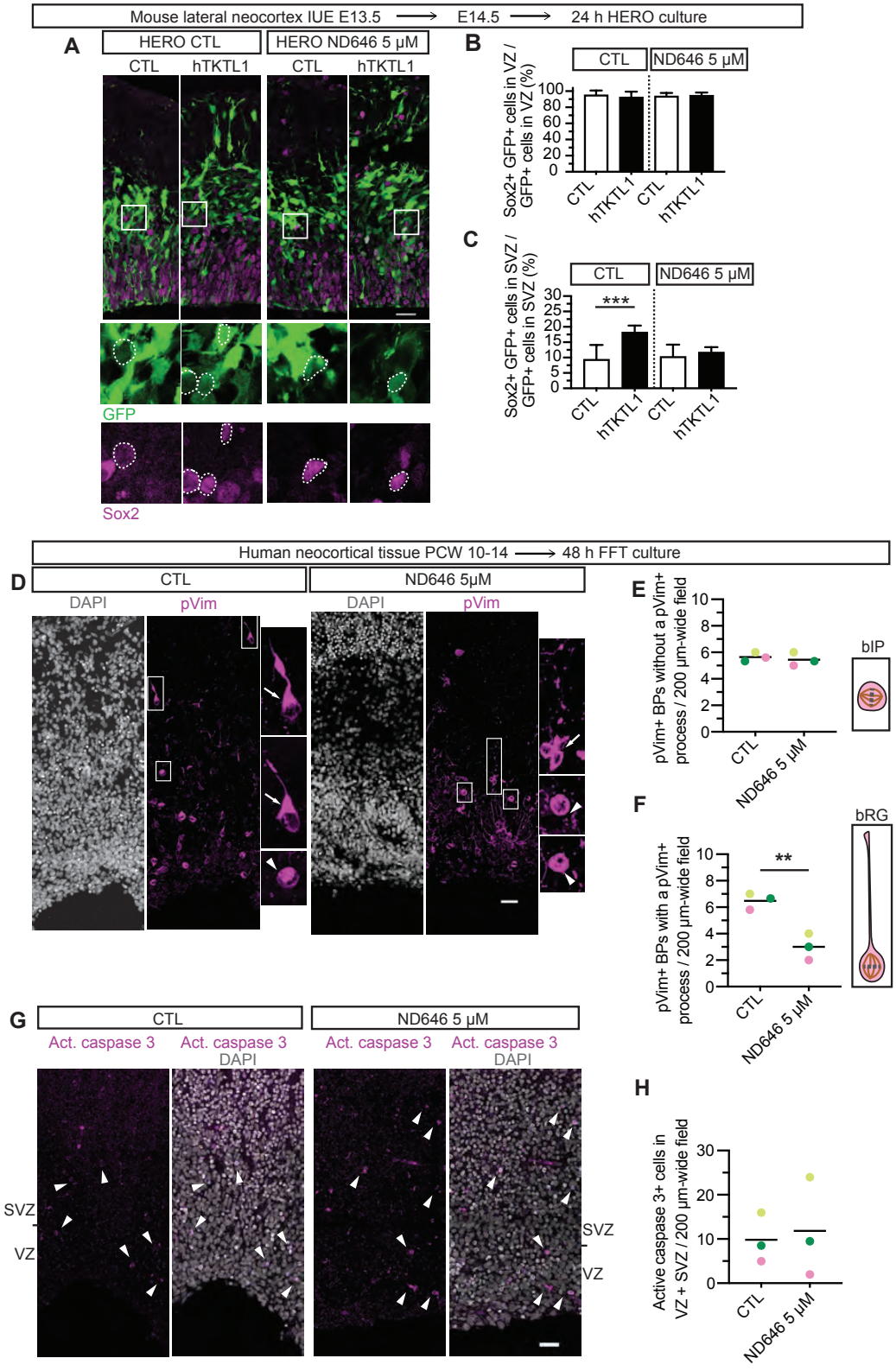
Mouse lateral neocortex IUE E13.5 ⟶ E14.5 ⟶ 24 h HERO culture
A
HERO CTL
HERO ND646 5 μM
CTL
hTKTL1
CTL
hTKTL1
GFP
Sox2
B
CTL
ND646 5 μM
Sox2+ GFP+ cells in VZ / GFP+ cells in VZ (%)
100
80
60
40
20
0
CTL
hTKTL1
CTL
hTKTL1
C
CTL
ND646 5 μM
Sox2+ GFP+ cells in SVZ / GFP+ cells in SVZ (%)
***
30
25
20
15
10
5
0
CTL
hTKTL1
CTL
hTKTL1
Human neocortical tissue PCW 10-14 ⟶ 48 h FFT culture
D
CTL
ND646 5μM
DAPI
pVim
DAPI
pVim
E
pVim+ BPs without a pVim+ process / 200 μm-wide field
10
8
6
4
2
0
CTL
ND646 5 μM
bIP
F
pVim+ BPs with a pVim+ process / 200 μm-wide field
**
10
8
6
4
2
0
CTL
ND646 5 μM
bRG
G
CTL
ND646 5 μM
Act. caspase 3
Act. caspase 3
DAPI
Act. caspase 3
Act. caspase 3
DAPI
SVZ
VZ
SVZ
VZ
H
Active caspase 3+ cells in VZ + SVZ / 200 μm-wide field
30
20
10
0
CTL
ND646 5 μM

Fig. S12. Inhibition of fatty acid synthesis by ND646 abolishes the hTKTL1-induced increase in bRG in embryonic mouse lateral neocortex and reduces bRG abundance, without affecting apoptosis, in fetal human neocortical tissue.

(**A-C**) Mouse lateral neocortex was electroporated *in utero* (IUE) at E13.5 with a pCAGGS plasmid encoding GFP, together with either an empty pCAGGS plasmid (control, CTL) or a plasmid encoding modern human TKTL1 (hTKTL1). The brain was dissected at E14.5 and the hemispheres were subjected to 24 hours of hemisphere rotation (HERO) culture in the absence (CTL) or presence of 5 μM of ND646, an inhibitor of acetyl-CoA carboxylase, followed by analyses.

(**A**) Immunofluorescence for GFP (green) and Sox2 (magenta) of cryosections of CTL– and hTKTL1–electroporated E14.5 mouse neocortex subjected to HERO culture for 24 hours without (CTL, left) or with (ND646, right) 5 μM ND646. White boxed areas in the SVZ are shown at higher magnification below the respective images. White dashed lines indicate Sox2+ GFP+ nuclei. Scale bar, 25 μm.

(**B, C**) Percentages of GFP+ cells in the VZ (B) and SVZ (C) that are Sox2+. Means of 4 to 8 embryos. Error bars, SD; Two-way ANOVA (B, C) with Bonferroni post-hoc test (C), (B) not significant, (C) *** $p < 0.001$.

(**D-H**) Human neocortical tissue (PCW 10-14) was subjected free-floating tissue (FFT) culture for 48 hours without (CTL) or with 5 μM ND646.

(**D**) Immunofluorescence of cryosections of PCW 10-14 fetal human neocortical tissue, subjected to FFT culture for 48 hours without (CTL, left) or with (ND646, right) 5 μM of ND646, for pVim (magenta) combined with DAPI staining (grey). White boxed areas in the SVZ are shown at higher magnification on the right side. Arrowheads indicate GFP+ pVim+ BPs without a process (mitotic bIPs). Arrows indicate GFP+ pVim+ BPs with a pVim+ process (mitotic bRG). Scale bar, 30 μm.

(**E, F**) Quantifications of pVim+ mitotic BPs without a pVim+ process (mitotic bIPs, as illustrated) (E) or with a pVim+ process (mitotic bRG, as illustrated) (F) in a 200 μm-wide field. Means of 3 different fetal samples, each of which is represented by a different color. Student's *t*-test, (E) not significant, (F) ** $p < 0.01$.

(**G**) Immunofluorescence of cryosections of PCW 10-14 fetal human neocortical tissue, subjected to FFT culture for 48 hours without (CTL, left) or with (ND646, right) 5 μM ND646, for active caspase 3 (magenta) combined with DAPI staining (grey). Arrowheads indicate active caspase 3+ cells. Scale bar, 30 μm.

(**H**) Quantification of active caspase 3+ cells in the VZ plus SVZ of a 200 μm-wide field. Means of 3 different fetal samples, each of which is represented by a different color. Student's *t*-test, not significant.

Fig. S13

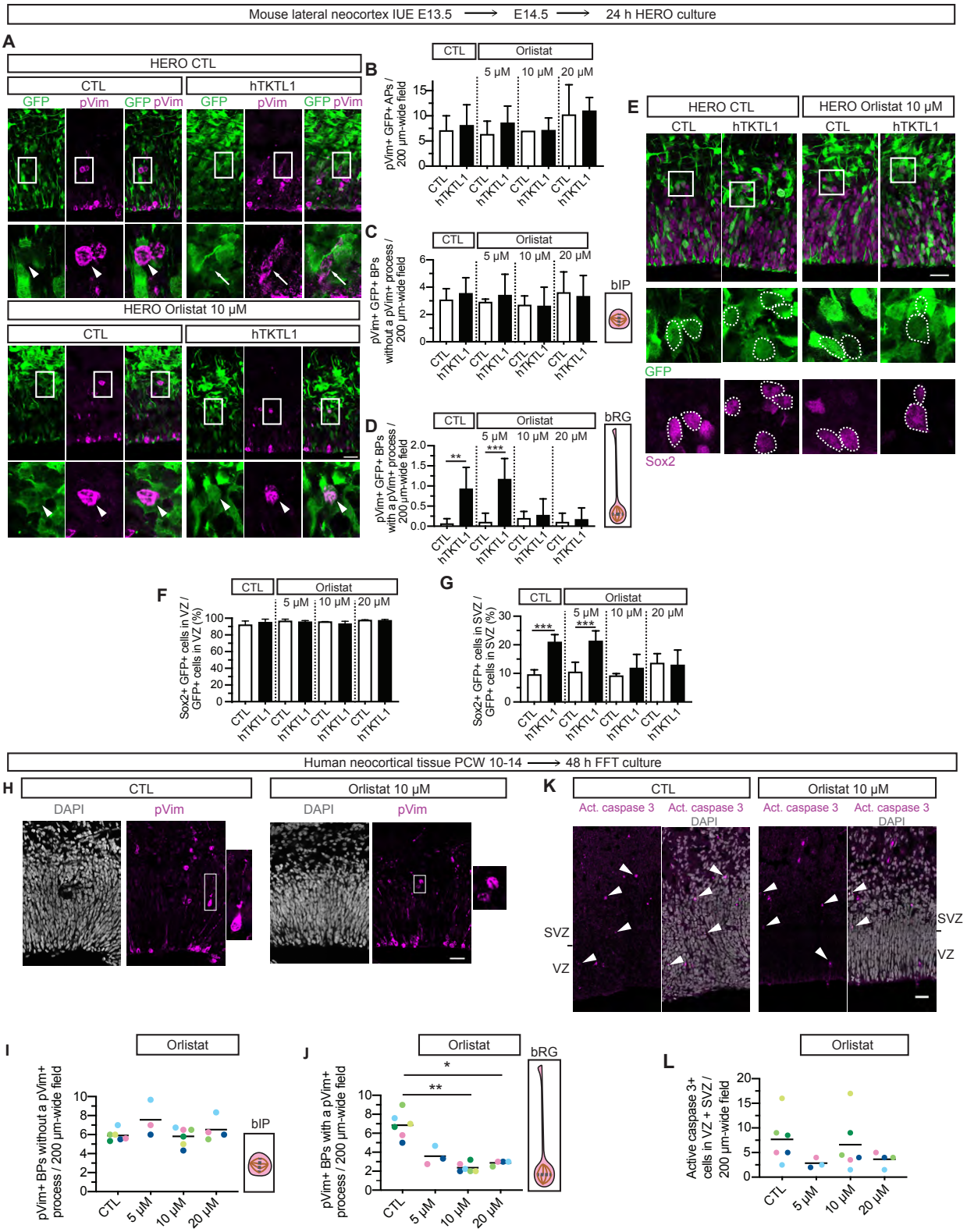
Mouse lateral neocortex IUE E13.5 ⟶ E14.5 ⟶ 24 h HERO culture
A
HERO CTL
CTL
hTKTL1
GFP
pVim
GFP pVim
HERO Orlistat 10 μM
B
CTL
Orlistat
5 μM
10 μM
20 μM
pVim+ GFP+ APs / 200 μm-wide field
C
pVim+ GFP+ BPs without a pVim+ process / 200 μm-wide field
bIP
D
pVim+ GFP+ BPs with a pVim+ process / 200 μm-wide field
bRG
E
HERO Orlistat 10 μM
GFP
Sox2
F
Sox2+ GFP+ cells in VZ / GFP+ cells in VZ (%)
G
Sox2+ GFP+ cells in SVZ / GFP+ cells in SVZ (%)
Human neocortical tissue PCW 10-14 ⟶ 48 h FFT culture
H
Orlistat 10 μM
DAPI
pVim
K
Act. caspase 3
SVZ
VZ
I
J
L
Active caspase 3+ cells in VZ + SVZ / 200 μm-wide field

Fig. S13. Inhibition of fatty acid synthesis by Orlistat abolishes the hTKTL1-induced increase in bRG in embryonic mouse lateral neocortex and reduces bRG abundance, without affecting apoptosis, in fetal human neocortical tissue.

(**A-G**) Mouse lateral neocortex was electroporated in utero (IUE) at E13.5 with a pCAGGS plasmid encoding GFP, together with either an empty pCAGGS plasmid (control, CTL) or a plasmid encoding modern human TKTL1 (hTKTL1). The brain was dissected at E14.5 and the hemispheres were subjected to 24 hours of hemisphere rotation (HERO) culture in the absence (CTL) or presence of 5, 10 or 20 μM of Orlistat, a fatty acid synthase inhibitor, followed by analyses.

(**A**) Immunofluorescence for GFP (green) and pVim (magenta) of cryosections of CTL– and hTKTL1–electroporated E14.5 mouse neocortex subjected to HERO culture for 24 hours without (CTL, top) or with (Orlistat, bottom) 10 μM Orlistat. White boxed areas in the SVZ are shown at higher magnification below the respective images. Arrowheads indicate GFP+ pVim+ BPs without a pVim+ process (mitotic bIPs). Arrows indicate a GFP+ pVim+ BP with a pVim+ process (mitotic bRG). Scale bar, 25 μm.

(**B-D**) Quantifications of pVim+ GFP+ mitotic (i) APs (B), (ii) BPs without a pVim+ process (mitotic bIPs, as illustrated) (C) and (iii) BPs with a pVim+ process (mitotic bRG, as illustrated) (D), in a 200 μm-wide field. Means of 3 to 7 embryos. Error bars, SD. Two-way ANOVA (B-D) with Bonferroni post-hoc test (D), (B, C) not significant, (D) ** $p < 0.01$, *** $p < 0.001$.

(**E**) Immunofluorescence for GFP (green) and Sox2 (magenta) of cryosections of CTL– and hTKTL1–electroporated E14.5 mouse neocortex subjected to HERO culture for 24 hours without (CTL, left) or with (Orlistat, right) 10 μM Orlistat. White boxed areas in the SVZ are shown at higher magnification below the respective images. White dashed lines indicate Sox2+ GFP+ nuclei. Scale bar, 25 μm.

(**F, G**) Percentages of GFP+ cells in the VZ (F) and SVZ (G) that are Sox2+. Means of 3 to 8 embryos. Error bars, SD. Two-way ANOVA (F, G) with Bonferroni post-hoc test (G), (F) not significant, (G) *** $p < 0.001$.

(**H-L**) Human neocortical tissue (PCW 10-14) was subjected free-floating tissue (FFT) culture for 48 hours without (CTL) or with (Orlistat) 5, 10 or 20 μM of Orlistat.

(**H**) Immunofluorescence of cryosections of PCW 10-14 fetal human neocortical tissue, subjected to FFT culture for 48 hours without (CTL, left) or with (Orlistat, right) 10 μM Orlistat, for pVim (magenta) combined with DAPI staining (grey). White boxed areas in the SVZ are shown at higher magnification on the right. Scale bar, 30 μm.

(**I, J**) Quantifications of pVim+ mitotic BPs without a pVim+ process (mitotic bIPs, as illustrated) (I) or with a pVim+ process (mitotic bRG, as illustrated) (J) in a 200 μm-wide field. Means of 3 to 6 different fetal samples, each of which is represented by a different color. One-way ANOVA (I, J) with Tukey post-hoc test (J), (I) not significant, (J) * $p < 0.05$, ** $p < 0.01$.

(**K**) Immunofluorescence of cryosections of PCW 10-14 fetal human neocortical tissue, subjected to FFT culture for 48 hours without (CTL, left) or with (Orlistat, right) 10 μM Orlistat, for active caspase 3 (magenta) combined with DAPI staining (grey). Arrowheads indicate active caspase 3+ cells. Scale bar, 30 μm.

(**L**) Quantification of active caspase 3+ cells in the VZ plus SVZ of a 200 μm-wide field. Means of 3 to 6 different fetal samples, each of which is represented by a different color. One-way ANOVA, not significant.

References and Notes

1. M. Breyl, Triangulating Neanderthal cognition: A tale of not seeing the forest for the trees. *Wiley Interdiscip. Rev. Cogn. Sci.* **12**, e1545 (2021). doi:10.1002/wcs.1545 Medline

2. D. L. Hoffmann, C. D. Standish, M. García-Diez, P. B. Pettitt, J. A. Milton, J. Zilhão, J. J. Alcolea-González, P. Cantalejo-Duarte, H. Collado, R. de Balbín, M. Lorblanchet, J. Ramos-Muñoz, G.-C. Weniger, A. W. G. Pike, U-Th dating of carbonate crusts reveals Neandertal origin of Iberian cave art. *Science* **359**, 912–915 (2018). doi:10.1126/science.aap7778 Medline

3. D. Leder, R. Hermann, M. Hüls, G. Russo, P. Hoelzmann, R. Nielbock, U. Böhner, J. Lehmann, M. Meier, A. Schwalb, A. Tröller-Reimer, T. Koddenberg, T. Terberger, A 51,000-year-old engraved bone reveals Neanderthals' capacity for symbolic behaviour. *Nat. Ecol. Evol.* **5**, 1273–1282 (2021). doi:10.1038/s41559-021-01487-z Medline

4. P. Rakic, Evolution of the neocortex: A perspective from developmental biology. *Nat. Rev. Neurosci.* **10**, 724–735 (2009). doi:10.1038/nrn2719 Medline

5. P. Gunz, A. K. Tilot, K. Wittfeld, A. Teumer, C. Y. Shapland, T. G. M. van Erp, M. Dannemann, B. Vernot, S. Neubauer, T. Guadalupe, G. Fernández, H. G. Brunner, W. Enard, J. Fallon, N. Hosten, U. Völker, A. Profico, F. Di Vincenzo, G. Manzi, J. Kelso, B. St Pourcain, J. J. Hublin, B. Franke, S. Pääbo, F. Macciardi, H. J. Grabe, S. E. Fisher, Neandertal introgression sheds light on modern human endocranial globularity. *Curr. Biol.* **29**, 120–127.e5 (2019). doi:10.1016/j.cub.2018.10.065 Medline

6. J. H. Lui, D. V. Hansen, A. R. Kriegstein, Development and evolution of the human neocortex. *Cell* **146**, 18–36 (2011). doi:10.1016/j.cell.2011.06.030 Medline

7. E. Taverna, M. Götz, W. B. Huttner, The cell biology of neurogenesis: Toward an understanding of the development and evolution of the neocortex. *Annu. Rev. Cell Dev. Biol.* **30**, 465–502 (2014). doi:10.1146/annurev-cellbio-101011-155801 Medline

8. I. Kelava, I. Reillo, A. Y. Murayama, A. T. Kalinka, D. Stenzel, P. Tomancak, F. Matsuzaki, C. Lebrand, E. Sasaki, J. C. Schwamborn, H. Okano, W. B. Huttner, V. Borrell, Abundant occurrence of basal radial glia in the subventricular zone of embryonic

neocortex of a lissencephalic primate, the common marmoset Callithrix jacchus. *Cereb. Cortex* **22**, 469–481 (2012). doi:10.1093/cercor/bhr301 Medline

9. X. Wang, J. W. Tsai, B. LaMonica, A. R. Kriegstein, A new subtype of progenitor cell in the mouse embryonic neocortex. *Nat. Neurosci.* **14**, 555–561 (2011). doi:10.1038/nn.2807 Medline

10. A. Shitamukai, D. Konno, F. Matsuzaki, Oblique radial glial divisions in the developing mouse neocortex induce self-renewing progenitors outside the germinal zone that resemble primate outer subventricular zone progenitors. *J. Neurosci.* **31**, 3683–3695 (2011). doi:10.1523/JNEUROSCI.4773-10.2011 Medline

11. M. Betizeau, V. Cortay, D. Patti, S. Pfister, E. Gautier, A. Bellemin-Ménard, M. Afanassieff, C. Huissoud, R. J. Douglas, H. Kennedy, C. Dehay, Precursor diversity and complexity of lineage relationships in the outer subventricular zone of the primate. *Neuron* **80**, 442–457 (2013). doi:10.1016/j.neuron.2013.09.032 Medline

12. S. A. Fietz, I. Kelava, J. Vogt, M. Wilsch-Bräuninger, D. Stenzel, J. L. Fish, D. Corbeil, A. Riehn, W. Distler, R. Nitsch, W. B. Huttner, OSVZ progenitors of human and ferret neocortex are epithelial-like and expand by integrin signaling. *Nat. Neurosci.* **13**, 690–699 (2010). doi:10.1038/nn.2553 Medline

13. D. V. Hansen, J. H. Lui, P. R. Parker, A. R. Kriegstein, Neurogenic radial glia in the outer subventricular zone of human neocortex. *Nature* **464**, 554–561 (2010). doi:10.1038/nature08845 Medline

14. V. Borrell, M. Götz, Role of radial glial cells in cerebral cortex folding. *Curr. Opin. Neurobiol.* **27**, 39–46 (2014). doi:10.1016/j.conb.2014.02.007 Medline

15. A. Pinson, W. B. Huttner, Neocortex expansion in development and evolution—from genes to progenitor cell biology. *Curr. Opin. Cell Biol.* **73**, 9–18 (2021). doi:10.1016/j.ceb.2021.04.008 Medline

16. J. F. Coy, S. Dübel, P. Kioschis, K. Thomas, G. Micklem, H. Delius, A. Poustka, Molecular cloning of tissue-specific transcripts of a transketolase-related gene: Implications for the evolution of new vertebrate genes. *Genomics* **32**, 309–316 (1996). doi:10.1006/geno.1996.0124 Medline

17. B. L. Horecker, The pentose phosphate pathway. *J. Biol. Chem.* **277**, 47965–47971 (2002). doi:10.1074/jbc.X200007200 Medline

18. J. F. Coy, D. Dressler, J. Wilde, P. Schubert, Mutations in the transketolase-like gene TKTL1: Clinical implications for neurodegenerative diseases, diabetes and cancer. *Clin. Lab.* **51**, 257–273 (2005). Medline

19. S. Diaz-Moralli, E. Aguilar, S. Marin, J. F. Coy, M. Dewerchin, M. R. Antoniewicz, O. Meca-Cortés, L. Notebaert, B. Ghesquière, G. Eelen, T. M. Thomson, P. Carmeliet, M. Cascante, A key role for transketolase-like 1 in tumor metabolic reprogramming. *Oncotarget* **7**, 51875–51897 (2016). doi:10.18632/oncotarget.10429 Medline

20. A. A. Pollen, T. J. Nowakowski, J. Chen, H. Retallack, C. Sandoval-Espinosa, C. R. Nicholas, J. Shuga, S. J. Liu, M. C. Oldham, A. Diaz, D. A. Lim, A. A. Leyrat, J. A. West, A. R. Kriegstein, Molecular identity of human outer radial glia during cortical development. *Cell* **163**, 55–67 (2015). doi:10.1016/j.cell.2015.09.004 Medline

21. S. A. Fietz, R. Lachmann, H. Brandl, M. Kircher, N. Samusik, R. Schröder, N. Lakshmanaperumal, I. Henry, J. Vogt, A. Riehn, W. Distler, R. Nitsch, W. Enard, S. Pääbo, W. B. Huttner, Transcriptomes of germinal zones of human and mouse fetal neocortex suggest a role of extracellular matrix in progenitor self-renewal. *Proc. Natl. Acad. Sci. U.S.A.* **109**, 11836–11841 (2012). doi:10.1073/pnas.1209647109 Medline

22. M. Florio, M. Albert, E. Taverna, T. Namba, H. Brandl, E. Lewitus, C. Haffner, A. Sykes, F. K. Wong, J. Peters, E. Guhr, S. Klemroth, K. Prüfer, J. Kelso, R. Naumann, I. Nüsslein, A. Dahl, R. Lachmann, S. Pääbo, W. B. Huttner, Human-specific gene ARHGAP11B promotes basal progenitor amplification and neocortex expansion. *Science* **347**, 1465–1470 (2015). doi:10.1126/science.aaa1975 Medline

23. M. B. Johnson, P. P. Wang, K. D. Atabay, E. A. Murphy, R. N. Doan, J. L. Hecht, C. A. Walsh, Single-cell analysis reveals transcriptional heterogeneity of neural progenitors in human cortex. *Nat. Neurosci.* **18**, 637–646 (2015). doi:10.1038/nn.3980 Medline

24. W. Sun, Y. Liu, C. A. Glazer, C. Shao, S. Bhan, S. Demokan, M. Zhao, M. A. Rudek, P. K. Ha, J. A. Califano, TKTL1 is activated by promoter hypomethylation and contributes to head and neck squamous cell carcinoma carcinogenesis through increased aerobic

glycolysis and HIF1α stabilization. *Clin. Cancer Res.* **16**, 857–866 (2010). doi:10.1158/1078-0432.CCR-09-2604 Medline

25. R. Peltonen, K. Ahopelto, J. Hagström, C. Böckelman, C. Haglund, H. Isoniemi, High TKTL1 expression as a sign of poor prognosis in colorectal cancer with synchronous rather than metachronous liver metastases. *Cancer Biol. Ther.* **21**, 826–831 (2020). doi:10.1080/15384047.2020.1803008 Medline

26. W. Yuan, S. Wu, J. Guo, Z. Chen, J. Ge, P. Yang, B. Hu, Z. Chen, Silencing of TKTL1 by siRNA inhibits proliferation of human gastric cancer cells in vitro and in vivo. *Cancer Biol. Ther.* **9**, 710–716 (2010). doi:10.4161/cbt.9.9.11431 Medline

27. K. Prüfer, F. Racimo, N. Patterson, F. Jay, S. Sankararaman, S. Sawyer, A. Heinze, G. Renaud, P. H. Sudmant, C. de Filippo, H. Li, S. Mallick, M. Dannemann, Q. Fu, M. Kircher, M. Kuhlwilm, M. Lachmann, M. Meyer, M. Ongyerth, M. Siebauer, C. Theunert, A. Tandon, P. Moorjani, J. Pickrell, J. C. Mullikin, S. H. Vohr, R. E. Green, I. Hellmann, P. L. F. Johnson, H. Blanche, H. Cann, J. O. Kitzman, J. Shendure, E. E. Eichler, E. S. Lein, T. E. Bakken, L. V. Golovanova, V. B. Doronichev, M. V. Shunkov, A. P. Derevianko, B. Viola, M. Slatkin, D. Reich, J. Kelso, S. Pääbo, The complete genome sequence of a Neanderthal from the Altai Mountains. *Nature* **505**, 43–49 (2014). doi:10.1038/nature12886 Medline

28. J. A. Miller, S.-L. Ding, S. M. Sunkin, K. A. Smith, L. Ng, A. Szafer, A. Ebbert, Z. L. Riley, J. J. Royall, K. Aiona, J. M. Arnold, C. Bennet, D. Bertagnolli, K. Brouner, S. Butler, S. Caldejon, A. Carey, C. Cuhaciyan, R. A. Dalley, N. Dee, T. A. Dolbeare, B. A. C. Facer, D. Feng, T. P. Fliss, G. Gee, J. Goldy, L. Gourley, B. W. Gregor, G. Gu, R. E. Howard, J. M. Jochim, C. L. Kuan, C. Lau, C.-K. Lee, F. Lee, T. A. Lemon, P. Lesnar, B. McMurray, N. Mastan, N. Mosqueda, T. Naluai-Cecchini, N.-K. Ngo, J. Nyhus, A. Oldre, E. Olson, J. Parente, P. D. Parker, S. E. Parry, A. Stevens, M. Pletikos, M. Reding, K. Roll, D. Sandman, M. Sarreal, S. Shapouri, N. V. Shapovalova, E. H. Shen, N. Sjoquist, C. R. Slaughterbeck, M. Smith, A. J. Sodt, D. Williams, L. Zöllei, B. Fischl, M. B. Gerstein, D. H. Geschwind, I. A. Glass, M. J. Hawrylycz, R. F. Hevner, H. Huang, A. R. Jones, J. A. Knowles, P. Levitt, J. W. Phillips, N. Šestan, P. Wohnoutka, C. Dang, A.

Bernard, J. G. Hohmann, E. S. Lein, Transcriptional landscape of the prenatal human brain. *Nature* **508**, 199–206 (2014). doi:10.1038/nature13185 Medline

29. S. Vaid, J. G. Camp, L. Hersemann, C. Eugster Oegema, A.-K. Heninger, S. Winkler, H. Brandl, M. Sarov, B. Treutlein, W. B. Huttner, T. Namba, A novel population of Hopx-dependent basal radial glial cells in the developing mouse neocortex. *Development* **145**, dev169276 (2018). doi:10.1242/dev.169276 Medline

30. M. A. Martínez-Martínez, C. De Juan Romero, V. Fernández, A. Cárdenas, M. Götz, V. Borrell, A restricted period for formation of outer subventricular zone defined by Cdh1 and Trnp1 levels. *Nat. Commun.* **7**, 11812 (2016). doi:10.1038/ncomms11812 Medline

31. N. Kalebic, C. Gilardi, B. Stepien, M. Wilsch-Bräuninger, K. R. Long, T. Namba, M. Florio, B. Langen, B. Lombardot, A. Shevchenko, M. W. Kilimann, H. Kawasaki, P. Wimberger, W. B. Huttner, Neocortical expansion due to increased proliferation of basal progenitors is linked to changes in their morphology. *Cell Stem Cell* **24**, 535–550.e9 (2019). doi:10.1016/j.stem.2019.02.017 Medline

32. N. Matsumoto, Y. Shinmyo, Y. Ichikawa, H. Kawasaki, Gyrification of the cerebral cortex requires FGF signaling in the mammalian brain. *eLife* **6**, e29285 (2017). doi:10.7554/eLife.29285 Medline

33. V. Fernández, C. Llinares-Benadero, V. Borrell, Cerebral cortex expansion and folding: What have we learned? *EMBO J.* **35**, 1021–1044 (2016). doi:10.15252/embj.201593701 Medline

34. J. S. Hothersall, M. Gordge, A. A. Noronha-Dutra, Inhibition of NADPH supply by 6-aminonicotinamide: Effect on glutathione, nitric oxide and superoxide in J774 cells. *FEBS Lett.* **434**, 97–100 (1998). doi:10.1016/S0014-5793(98)00959-4 Medline

35. V. Stepanova, K. E. Moczulska, G. N. Vacano, I. Kurochkin, X. Ju, S. Riesenberg, D. Macak, T. Maricic, L. Dombrowski, M. Schörnig, K. Anastassiadis, O. Baker, R. Naumann, E. Khrameeva, A. Vanushkina, E. Stekolshchikova, A. Egorova, A. Tkachev, R. Mazzarino, N. Duval, D. Zubkov, P. Giavalisco, T. G. Wilkinson, D. Patterson, P. Khaitovich, S. Pääbo, Reduced purine biosynthesis in humans after their divergence from Neandertals. *eLife* **10**, e58741 (2021). doi:10.7554/eLife.58741 Medline

36. C. A. Trujillo, E. S. Rice, N. K. Schaefer, I. A. Chaim, E. C. Wheeler, A. A. Madrigal, J. Buchanan, S. Preissl, A. Wang, P. D. Negraes, R. A. Szeto, R. H. Herai, A. Huseynov, M. S. A. Ferraz, F. S. Borges, A. H. Kihara, A. Byrne, M. Marin, C. Vollmers, A. N. Brooks, J. D. Lautz, K. Semendeferi, B. Shapiro, G. W. Yeo, S. E. P. Smith, R. E. Green, A. R. Muotri, Reintroduction of the archaic variant of *NOVA1* in cortical organoids alters neurodevelopment. *Science* **371**, eaax2537 (2021). doi:10.1126/science.aax2537 Medline

37. T. Maricic, N. Helmbrecht, S. Riesenberg, D. Macak, P. Kanis, M. Lackner, A. D. Pugach-Matveeva, S. Pääbo, Comment on "Reintroduction of the archaic variant of *NOVA1* in cortical organoids alters neurodevelopment". *Science* **374**, eabi6060 (2021). doi:10.1126/science.abi6060 Medline

38. T. Namba, J. Nardelli, P. Gressens, W. B. Huttner, Metabolic regulation of neocortical expansion in development and evolution. *Neuron* **109**, 408–419 (2021). doi:10.1016/j.neuron.2020.11.014 Medline

39. T. Namba, J. Dóczi, A. Pinson, L. Xing, N. Kalebic, M. Wilsch-Bräuninger, K. R. Long, S. Vaid, J. Lauer, A. Bogdanova, B. Borgonovo, A. Shevchenko, P. Keller, D. Drechsel, T. Kurzchalia, P. Wimberger, C. Chinopoulos, W. B. Huttner, Human-specific ARHGAP11B acts in mitochondria to expand neocortical progenitors by glutaminolysis. *Neuron* **105**, 867–881.e9 (2020). doi:10.1016/j.neuron.2019.11.027 Medline

40. M. Florio, T. Namba, S. Pääbo, M. Hiller, W. B. Huttner, A single splice site mutation in human-specific *ARHGAP11B* causes basal progenitor amplification. *Sci. Adv.* **2**, e1601941 (2016). doi:10.1126/sciadv.1601941 Medline

41. F. Röhrig, A. Schulze, The multifaceted roles of fatty acid synthesis in cancer. *Nat. Rev. Cancer* **16**, 732–749 (2016). doi:10.1038/nrc.2016.89 Medline

42. M. Bastir, A. Rosas, D. E. Lieberman, P. O'Higgins, Middle cranial fossa anatomy and the origin of modern humans. *Anat. Rec.* **291**, 130–140 (2008). doi:10.1002/ar.20636 Medline

43. S. Herculano-Houzel, The remarkable, yet not extraordinary, human brain as a scaled-up primate brain and its associated cost. *Proc. Natl. Acad. Sci. U.S.A.* **109** (suppl. 1), 10661–10668 (2012). doi:10.1073/pnas.1201895109 Medline

44. N. Kalebic, C. Gilardi, M. Albert, T. Namba, K. R. Long, M. Kostic, B. Langen, W. B. Huttner, Human-specific *ARHGAP11B* induces hallmarks of neocortical expansion in developing ferret neocortex. *eLife* **7**, e41241 (2018). doi:10.7554/eLife.41241 Medline

45. J. Schenk, M. Wilsch-Bräuninger, F. Calegari, W. B. Huttner, Myosin II is required for interkinetic nuclear migration of neural progenitors. *Proc. Natl. Acad. Sci. U.S.A.* **106**, 16487–16492 (2009). doi:10.1073/pnas.0908928106 Medline

46. K. R. Long, B. Newland, M. Florio, N. Kalebic, B. Langen, A. Kolterer, P. Wimberger, W. B. Huttner, Extracellular matrix components HAPLN1, lumican, and collagen I cause hyaluronic acid-dependent folding of the developing human neocortex. *Neuron* **99**, 702–719.e6 (2018). doi:10.1016/j.neuron.2018.07.013 Medline

47. M. A. Lancaster, J. A. Knoblich, Generation of cerebral organoids from human pluripotent stem cells. *Nat. Protoc.* **9**, 2329–2340 (2014). doi:10.1038/nprot.2014.158 Medline

48. F. Mora-Bermúdez, F. Badsha, S. Kanton, J. G. Camp, B. Vernot, K. Köhler, B. Voigt, K. Okita, T. Maricic, Z. He, R. Lachmann, S. Pääbo, B. Treutlein, W. B. Huttner, Differences and similarities between human and chimpanzee neural progenitors during cerebral cortex development. *eLife* **5**, e18683 (2016). doi:10.7554/eLife.18683 Medline

49. S. Elf, R. Lin, S. Xia, Y. Pan, C. Shan, S. Wu, S. Lonial, M. Gaddh, M. L. Arellano, H. J. Khoury, F. R. Khuri, B. H. Lee, T. J. Boggon, J. Fan, J. Chen, Targeting 6-phosphogluconate dehydrogenase in the oxidative PPP sensitizes leukemia cells to antimalarial agent dihydroartemisinin. *Oncogene* **36**, 254–262 (2017). doi:10.1038/onc.2016.196 Medline

50. A. Herms, M. Bosch, B. J. N. Reddy, N. L. Schieber, A. Fajardo, C. Rupérez, A. Fernández-Vidal, C. Ferguson, C. Rentero, F. Tebar, C. Enrich, R. G. Parton, S. P. Gross, A. Pol, AMPK activation promotes lipid droplet dispersion on detyrosinated microtubules to increase mitochondrial fatty acid oxidation. *Nat. Commun.* **6**, 7176 (2015). doi:10.1038/ncomms8176 Medline

51. E. Q. Li, W. Zhao, C. Zhang, L.-Z. Qin, S.-J. Liu, Z.-Q. Feng, X. Wen, C.-P. Chen, Synthesis and anti-cancer activity of ND-646 and its derivatives as acetyl-CoA carboxylase 1

inhibitors. *Eur. J. Pharm. Sci.* **137**, 105010 (2019). doi:10.1016/j.ejps.2019.105010 Medline

52. M. Knobloch, S. M. G. Braun, L. Zurkirchen, C. von Schoultz, N. Zamboni, M. J. Araúzo-Bravo, W. J. Kovacs, O. Karalay, U. Suter, R. A. C. Machado, M. Roccio, M. P. Lutolf, C. F. Semenkovich, S. Jessberger, Metabolic control of adult neural stem cell activity by Fasn-dependent lipogenesis. *Nature* **493**, 226–230 (2013). doi:10.1038/nature11689 Medline

53. N. Kalebic, E. Taverna, S. Tavano, F. K. Wong, D. Suchold, S. Winkler, W. B. Huttner, M. Sarov, CRISPR/Cas9-induced disruption of gene expression in mouse embryonic brain and single neural stem cells in vivo. *EMBO Rep.* **17**, 338–348 (2016). doi:10.15252/embr.201541715 Medline

54. S. Riesenberg, M. Chintalapati, D. Macak, P. Kanis, T. Maricic, S. Pääbo, Simultaneous precise editing of multiple genes in human cells. *Nucleic Acids Res.* **47**, e116 (2019). doi:10.1093/nar/gkz669 Medline

55. I. Weisheit, J. A. Kroeger, R. Malik, J. Klimmt, D. Crusius, A. Dannert, M. Dichgans, D. Paquet, Detection of deleterious on-target effects after HDR-mediated CRISPR editing. *Cell Rep.* **31**, 107689 (2020). doi:10.1016/j.celrep.2020.107689 Medline

56. M. Florio, M. Heide, A. Pinson, H. Brandl, M. Albert, S. Winkler, P. Wimberger, W. B. Huttner, M. Hiller, Evolution and cell-type specificity of human-specific genes preferentially expressed in progenitors of fetal neocortex. *eLife* **7**, e32332 (2018). doi:10.7554/eLife.32332 Medline

57. L. Xing, A. Kubik-Zahorodna, T. Namba, A. Pinson, M. Florio, J. Prochazka, M. Sarov, R. Sedlacek, W. B. Huttner, Expression of human-specific ARHGAP11B in mice leads to neocortex expansion and increased memory flexibility. *EMBO J.* **40**, e107093 (2021). doi:10.15252/embj.2020107093 Medline